



## RESEARCH ARTICLE

10.1002/2016MS000817

## Key Points:

- A biogeochemical model has been improved to simulate relative importance of CH<sub>4</sub> production pathways and stable carbon (C) isotopic dynamics
- The ability to model stable C isotopic dynamics can better constrain simulations of the individual processes in CH<sub>4</sub> transformations
- The model has been tested against the observed CH<sub>4</sub> fluxes, CH<sub>4</sub> production pathways, and C isotopic signature of CH<sub>4</sub> in a northern peatland

## Correspondence to:

J. Deng,  
Jia.Deng@unh.edu

## Citation:

Deng, J., et al. (2017), Adding stable carbon isotopes improves model representation of the role of microbial communities in peatland methane cycling, *J. Adv. Model. Earth Syst.*, 9, 1412–1430, doi:10.1002/2016MS000817.

Received 26 SEP 2016

Accepted 5 MAY 2017

Accepted article online 12 MAY 2017

Published online 13 JUN 2017

## Adding stable carbon isotopes improves model representation of the role of microbial communities in peatland methane cycling

Jia Deng<sup>1</sup> , Carmody K McCalley<sup>2</sup> , Steve Frolking<sup>1</sup>, Jeff Chanton<sup>3</sup> , Patrick Crill<sup>4</sup> , Ruth Varner<sup>1,5</sup> , Gene Tyson<sup>6</sup>, Virginia Rich<sup>7</sup> , Mark Hines<sup>8</sup>, Scott R. Saleska<sup>9</sup>, and Changsheng Li<sup>1</sup>

<sup>1</sup>Earth Systems Research Center, Institute for the Study of Earth, Oceans and Space, University of New Hampshire, Durham, New Hampshire, USA, <sup>2</sup>Thomas H. Gosnell School of Life Sciences, Rochester Institute of Technology, One Lomb Memorial Drive, Rochester, New York, USA, <sup>3</sup>Department of Earth, Ocean and Atmospheric Science, Florida State University, Tallahassee, Florida, USA, <sup>4</sup>Department of Geological Sciences, Stockholm University, Stockholm, Sweden, <sup>5</sup>Department of Earth Sciences, University of New Hampshire, Durham, New Hampshire, USA, <sup>6</sup>Australian Centre for Ecogenomics, School of Chemistry and Molecular Biosciences, University of Queensland, Brisbane, Queensland, Australia, <sup>7</sup>Department of Microbiology, The Ohio State University, Columbus, Ohio, USA, <sup>8</sup>Department of Biological Sciences, University of Massachusetts Lowell, Lowell, Massachusetts, USA, <sup>9</sup>Department of Ecology and Evolutionary Biology, University of Arizona, Tucson, Arizona, USA

**Abstract** Climate change is expected to have significant and uncertain impacts on methane (CH<sub>4</sub>) emissions from northern peatlands. Biogeochemical models can extrapolate site-specific CH<sub>4</sub> measurements to larger scales and predict responses of CH<sub>4</sub> emissions to environmental changes. However, these models include considerable uncertainties and limitations in representing CH<sub>4</sub> production, consumption, and transport processes. To improve predictions of CH<sub>4</sub> transformations, we incorporated acetate and stable carbon (C) isotopic dynamics associated with CH<sub>4</sub> cycling into a biogeochemistry model, DNDC. By including these new features, DNDC explicitly simulates acetate dynamics and the relative contribution of acetotrophic and hydrogenotrophic methanogenesis (AM and HM) to CH<sub>4</sub> production, and predicts the C isotopic signature ( $\delta^{13}\text{C}$ ) in soil C pools and emitted gases. When tested against biogeochemical and microbial community observations at two sites in a zone of thawing permafrost in a subarctic peatland in Sweden, the new formulation substantially improved agreement with CH<sub>4</sub> production pathways and  $\delta^{13}\text{C}$  in emitted CH<sub>4</sub> ( $\delta^{13}\text{C-CH}_4$ ), a measure of the integrated effects of microbial production and consumption, and of physical transport. We also investigated the sensitivity of simulated  $\delta^{13}\text{C-CH}_4$  to C isotopic composition of substrates and, to fractionation factors for CH<sub>4</sub> production ( $\alpha_{\text{AM}}$  and  $\alpha_{\text{HM}}$ ), CH<sub>4</sub> oxidation ( $\alpha_{\text{MO}}$ ), and plant-mediated CH<sub>4</sub> transport ( $\alpha_{\text{TP}}$ ). The sensitivity analysis indicated that the  $\delta^{13}\text{C-CH}_4$  is highly sensitive to the factors associated with microbial metabolism ( $\alpha_{\text{AM}}$ ,  $\alpha_{\text{HM}}$ , and  $\alpha_{\text{MO}}$ ). The model framework simulating stable C isotopic dynamics provides a robust basis for better constraining and testing microbial mechanisms in predicting CH<sub>4</sub> cycling in peatlands.

### 1. Introduction

Northern peatlands are characterized by cold, wet conditions that promote the sequestration of atmospheric carbon dioxide (CO<sub>2</sub>) into surface soil organic carbon (SOC) or peat [e.g., Gorham, 1991; Zimov *et al.*, 2006; Schuur *et al.*, 2008]. These peatlands have accumulated 473–621 Pg (10<sup>15</sup> g) carbon (C) since the Last Glacial Maximum [Yu *et al.*, 2010], with more than 277 Pg C stored in permafrost areas [Schuur *et al.*, 2008; Tarnocai *et al.*, 2009]. Although northern peatlands are currently a net C sink, they are an important source of atmospheric methane (CH<sub>4</sub>), releasing 31–65 Tg (10<sup>12</sup> g) CH<sub>4</sub> yr<sup>-1</sup> [McGuire *et al.*, 2009]. Recent studies indicate that the rate and extent of permafrost degradation is increasing with pronounced climate warming in northern peatlands [e.g., James *et al.*, 2013; Payette *et al.*, 2004; Quinton *et al.*, 2011; Åkerman and Johansson, 2008]. Permafrost thaw can result in changes in topography (e.g., thermokarst), soil climate, and vegetation [e.g., Avis *et al.*, 2011; Malmier *et al.*, 2005; Schuur *et al.*, 2008]. Changes associated with climate warming and permafrost degradation mobilizes previously frozen C, and stimulates microbial decomposition of peat C stocks into the climate forcing trace gases CO<sub>2</sub> and CH<sub>4</sub> [e.g., Dorrepaal *et al.*, 2009; Frolking *et al.*, 2011; Johnston *et al.*, 2014; McGuire *et al.*, 2009; Schuur *et al.*, 2009, 2011]. Increased emissions of C gases, CH<sub>4</sub> in

© 2017. The Authors.

This is an open access article under the terms of the Creative Commons Attribution-NonCommercial-NoDerivs License, which permits use and distribution in any medium, provided the original work is properly cited, the use is non-commercial and no modifications or adaptations are made.

particular due to its strong global warming potential (28 kg CO<sub>2</sub>-equivalents kg<sup>-1</sup> CH<sub>4</sub> at a 100 year time-scale) [IPCC, 2013], would increase the rate of warming, forming a significant positive biogeochemical feedback to climate [e.g., Olefeldt *et al.*, 2013].

Despite considerable research attention focused on CH<sub>4</sub> emissions from northern peatlands, large uncertainty over their magnitude and variability remains [e.g., Limpens *et al.*, 2008; McGuire *et al.*, 2009; Olefeldt *et al.*, 2013]. Northern peatlands are highly heterogeneous, usually with varying characteristics of permafrost, topography, hydrology, soil, and vegetation within close proximity [Eppinga *et al.*, 2009], which results in considerable variations of CH<sub>4</sub> fluxes at local and landscape scales [e.g., Bäckstrand *et al.*, 2010; Lund *et al.*, 2010; Sachs *et al.*, 2010]. To extrapolate site-specific CH<sub>4</sub> measurements to larger regions and/or predict responses of CH<sub>4</sub> emissions to environmental changes, process-based biogeochemical models have been developed and applied from site to global scales [e.g., Wania *et al.*, 2013; Melton *et al.*, 2013; Xu *et al.*, 2016]. While many improvements have been made in modeling CH<sub>4</sub> emissions from northern areas by incorporating thermal, hydrologic, vegetation, and biogeochemical processes in relation to permafrost characteristics into model frameworks [e.g., Schneider von Diemling *et al.*, 2012; Wania *et al.*, 2009a, 2009b; Zhuang *et al.*, 2001, 2004], key limitations and uncertainties still exist. There are a number of important controls over CH<sub>4</sub> production, consumption, and transport that have not been, or are inadequately, incorporated into existing CH<sub>4</sub> biogeochemical models [Bridgham *et al.*, 2013].

For example, most existing models use net primary production or SOC as an index to represent substrate availability for CH<sub>4</sub> production and do not differentiate CH<sub>4</sub> production pathways, i.e., acetotrophic methanogenesis (AM) and hydrogenotrophic methanogenesis (HM), although mechanisms of CH<sub>4</sub> production are usually addressed differently in the models [Bridgham *et al.*, 2013; Melton *et al.*, 2013; Xu *et al.*, 2016]. In addition, the ability to test model simulations of the individual processes of CH<sub>4</sub> production, oxidation, and transport is still limited because only a few model parameters and/or processes can be constrained by comparing models against measurements of net CH<sub>4</sub> emissions [Bridgham *et al.*, 2013].

The process-based biogeochemical model, DeNitrification-DeComposition (DNDC), incorporates both the AM and HM pathways for CH<sub>4</sub> production [Fumoto *et al.*, 2008], and has a permafrost thermal submodel, based on the Northern Ecosystem Soil Temperature (NEST) model, in order to simulate high-latitude soil biogeochemistry in permafrost ecosystems, and has been tested against CH<sub>4</sub> flux data measured at several northern peatlands [Deng *et al.*, 2014, 2015; Zhang *et al.*, 2012]. However, new data characterizing the methanogen community at Stordalen Mire in Sweden indicate that HM lineages dominate the methanogen community in early thaw stages [McCalley *et al.*, 2014; Mondav *et al.*, 2014] whereas DNDC simulations show primarily AM. Given the importance of this microbially mediated process in regulating CH<sub>4</sub> dynamics across the permafrost thaw gradient [McCalley *et al.*, 2014], this discrepancy in simulating CH<sub>4</sub> production pathway may hinder reliable prediction of responses of CH<sub>4</sub> emissions to permafrost degradation. Since different CH<sub>4</sub>-cycling microbes fractionate <sup>13</sup>C differently [Conrad, 2005], adding stable C isotopic information to soil organic C processing in DNDC is a potentially powerful tool for generating predictions, based on microbial CH<sub>4</sub>-cycling mechanisms, that can be tested against observations of the <sup>13</sup>C isotopic composition of emitted gases. High temporal frequency measurements of the magnitude and isotopic composition of CH<sub>4</sub> emissions have been made at Stordalen Mire on plots with and without permafrost [McCalley *et al.*, 2014], providing an excellent case study.

To address both the simulation discrepancy of AM versus HM production and uncertainty in the description of the net flux versus individual processes of CH<sub>4</sub> production, oxidation, and transport, we made two significant modifications to DNDC simulations of CH<sub>4</sub> cycling. First, stable C isotopic values of soil C pools and fractionation impacts of C processing pathways were added to the model. Second, the anaerobic fermentation pathway in DNDC was modified to include the production of an intermediate pool—acetate—which can be consumed in AM or by oxidation by other terminal electron acceptors. In this study, we report the details of these modifications, a sensitivity assessment, and evaluation of the new model formulation against field data from Stordalen Mire.

## 2. The Study Area and Field Data

Field data used for this study were collected at a subarctic peatland with discontinuous, ice-rich permafrost, Stordalen Mire, (68°20'N, 19°03'E, 351 m.a.s.l.) located 10 km southeast of the Abisko Scientific Research

Station (ANS) in northern Sweden. This area has a continental climate, with an annual mean air temperature of 0.07°C and an average annual precipitation of 308 mm [Bäckstrand *et al.*, 2008]. The annual mean air temperature at Abisko has increased by 2.5°C from 1913 to 2006, significantly exceeding the 0°C threshold for the first time during the last few decades [Callaghan *et al.*, 2010]. The warming has led to a thicker active layer and some permafrost disappearance in this area [Åkerman and Johansson, 2008]. The degradation of permafrost has significantly affected topography, hydrology, soil environment, and vegetation, and thereby exerted a strong influence on the fluxes of C gases [Christensen *et al.*, 2004; Johansson *et al.*, 2006; Malmer *et al.*, 2005; Åkerman and Johansson, 2008; Bäckstrand *et al.*, 2008; McCalley *et al.*, 2014].

As in most peatlands in discontinuous permafrost regions, Stordalen Mire has high spatial heterogeneity in topography (1–2 m relative differences in elevation). The variability of topography creates spatially restricted environments (on the scale of m<sup>2</sup>) with different soil moisture and nutrient conditions that support different plant communities [Rosswall *et al.*, 1975; Bäckstrand *et al.*, 2008]. Measurements at Stordalen Mire have been made at three sites that represent three dominant cover types, Palsa, Sphagnum, and Eriophorum (note that in this study the terms Sphagnum and Eriophorum are used to denote land cover types instead of vegetation species, though the site terms are derived from the dominant vegetation). The Palsa sites are dry features underlain by permafrost, with an active layer thickness (ALT; the thickness of the surface soil layer that freezes and thaws seasonally above a year-round frozen layer) usually <0.7 m in late summer. The Sphagnum sites are partially underlain by permafrost, representing intermediate thaw features, with an ALT generally thicker than 1.0 m in late summer and water table levels fluctuating within 0–25 cm below the ground surface. The plant community structure, the fluctuating water table, and the pore water chemistry indicate that they are ombrotrophic, perched above the local water table. The Eriophorum sites have no detectable permafrost and are generally wetter than Sphagnum, with water table levels generally at or above the peat surface [Bäckstrand *et al.*, 2008, 2010; Olefeldt and Roulet, 2012], and are minerotrophic. During the last several decades, there have been pronounced shifts in the extent of these three land cover types, with some drier sites getting wetter and shifting vegetation cover as permafrost thaws [Christensen *et al.*, 2004; Malmer *et al.*, 2005]. These three land cover types can be regarded as representing a natural landscape gradient of permafrost thaw [e.g., Malmer *et al.*, 2005; Johansson *et al.*, 2006; Bäckstrand *et al.*, 2010; Hodgkins *et al.*, 2014, 2015].

There are multiyear field records of CO<sub>2</sub> and CH<sub>4</sub> fluxes at Stordalen, measured using automated chambers. In a previous study, we validated the DNDC model against the multiyear (2003–2009) field records, including soil freeze/thaw dynamics, NEE, and CH<sub>4</sub> fluxes, and the validation indicated that DNDC was able to simulate the observed differences in seasonal soil thaw, NEE, and CH<sub>4</sub> fluxes across the three cover types [Deng *et al.*, 2014].

Since 2011, additional field studies have been conducted at Stordalen with a focus on measuring the role of microbial communities in regulating CH<sub>4</sub> dynamics [Hodgkins *et al.*, 2014; McCalley *et al.*, 2014; Mondav *et al.*, 2014]. Daily averaged values of CH<sub>4</sub> flux rates and δ<sup>13</sup>C of emitted CH<sub>4</sub> were derived from frequent (subdaily) measurements made at the Sphagnum and Eriophorum sites from 2011 to 2013 using a Quantum Cascade Laser Spectrometer (QCLS, Aerodyne Research Inc.) connected to an automated chamber system [McCalley *et al.*, 2014]. The relative abundance of methanogens was also quantified in peat collected near the auto chambers four times through the 2011 growing season (15 June, 12 July, 15 August, and 15 October) using 16S rRNA gene amplicon sequencing (described in detail in McCalley *et al.* [2014] and Mondav *et al.* [2014]). In addition, soil water table depth (WTD, positive values up from the ground surface) was measured three to five times per week from June to October each year [McCalley *et al.*, 2014]. Daily meteorological data, including air temperature, precipitation, solar radiation, wind speed, and relative humidity, were recorded at ANS (Figure 1).

The field data indicated that: (1) CH<sub>4</sub> fluxes and isotopic composition were significantly different between the study sites, with an increasing trend for both CH<sub>4</sub> fluxes and δ<sup>13</sup>C-CH<sub>4</sub> with permafrost thaw, (2) CH<sub>4</sub> production pathways were different between the sites and a distinct shift from HM to AM was observed along the thaw gradient, and (3) microbial community and CH<sub>4</sub> production pathway played an important role in regulating CH<sub>4</sub> dynamics at Stordalen Mire, and could be crucial for improving model predictions of CH<sub>4</sub> feedbacks in response to climate change and permafrost thaw [McCalley *et al.*, 2014; Mondav *et al.*, 2014]. Driven by the discrepancies between the simulated and observed relative contributions of different

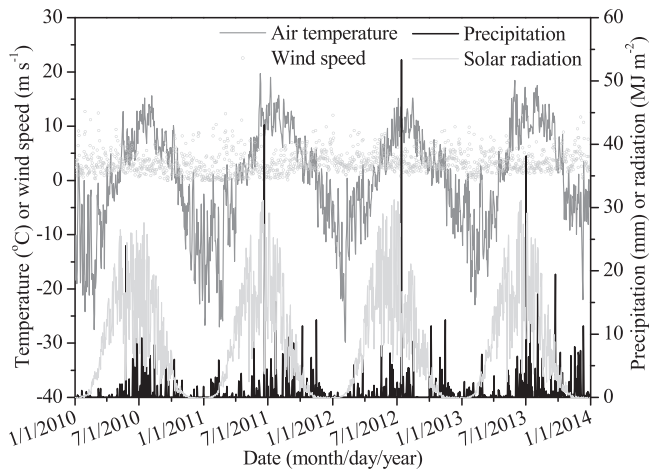


**Figure 1.** Daily average air temperature, wind speed, precipitation, and solar radiation during 2010–2013. Data were recorded at the Abisko Scientific Research Station (ANS).

DNDC is comprised of three major interacting submodels: soil climate, plant growth, and soil biogeochemistry. The soil climate and plant growth submodels convert the primary drivers, such as climate, soil properties, vegetation, and anthropogenic activity, into soil environmental factors, such as soil temperature and moisture, pH, redox potential (Eh), and substrate concentrations. The soil biogeochemistry submodel, including processes of decomposition, nitrification, denitrification, and fermentation, simulate C and N transformations that are mediated by soil microbes and controlled by soil environmental factors [Li, 2000; Li et al., 2012].

In DNDC, the rate of CH<sub>4</sub> emission is predicted by modeling its production, consumption, and transport processes. Production is simulated by calculating substrate concentrations (i.e., electron donors and acceptors) resulting from decomposition of SOC as well as plant root activities including exudation and respiration, and then by tracking a series of reductive reactions between electron donors (i.e., H<sub>2</sub> and dissolved organic carbon (DOC)) and acceptors (i.e., NO<sub>3</sub><sup>-</sup>, Mn<sup>4+</sup>, Fe<sup>3+</sup>, SO<sub>4</sub><sup>2-</sup>, and CO<sub>2</sub>). SOC decomposition is simulated by disaggregating SOC into four pools (i.e., litter, microbes, humads, and passive humus), and each pool is further divided into two or three subpools with specific C:N ratios and decomposition rates. During decomposition of each SOC subpool, the model distributes a fixed fraction of the released C into DOC [Li et al., 1992a]. DOC from SOC decomposition therefore depends on size and specific decomposition rate of each SOC pool, as well as soil thermal and moisture conditions [Li et al., 1992a, 2012]. DOC from root exudation is simulated as 45% of the C transferred to roots from photosynthetic production [Zhang et al., 2002]. When a soil is shifting from unsaturated to saturated conditions, soil oxygen is gradually depleted and additional oxidants (e.g., NO<sub>3</sub><sup>-</sup>, Mn<sup>4+</sup>, Fe<sup>3+</sup>, SO<sub>4</sub><sup>2-</sup>, and CO<sub>2</sub>) may become involved in reductive reactions. Soil Eh gradually decreases along with the consumption of these oxidants and DNDC simulates denitrification, reductions of Mn<sup>4+</sup>, Fe<sup>3+</sup>, and SO<sub>4</sub><sup>2-</sup>, and methane production as consecutive reactions with each reaction occurring under certain Eh conditions [Li et al., 2004]. The model simulates sequential reactions from NO<sub>3</sub><sup>-</sup> to N<sub>2</sub> in denitrification and calculates the rate of each step based on the concentrations of the corresponding nitrogenous oxides and DOC [Li et al., 1992a]. Reductions of Mn<sup>4+</sup>, Fe<sup>3+</sup>, and SO<sub>4</sub><sup>2-</sup> were simulated using dual-substrate Michaelis-Menten-based equations. Maximum rates for Mn<sup>4+</sup>, Fe<sup>3+</sup>, and SO<sub>4</sub><sup>2-</sup> reductions are set as 0.108 mol kg<sup>-1</sup> d<sup>-1</sup>, 0.108 mol kg<sup>-1</sup> d<sup>-1</sup>, and 0.691 mol m<sup>-3</sup> d<sup>-1</sup>, respectively. Michaelis-Menten half-saturation constants for Mn<sup>4+</sup>, Fe<sup>3+</sup>, and SO<sub>4</sub><sup>2-</sup> are 0.15 mol kg<sup>-1</sup>, 0.15 mol kg<sup>-1</sup>, and 0.23 mol m<sup>-3</sup>, respectively [Fumoto et al., 2008]. Michaelis-Menten half-saturation constants for DOC and H<sub>2</sub> are 0.46 mol m<sup>-3</sup> and 0.22 mmol m<sup>-3</sup>, respectively, for the Mn<sup>4+</sup> or Fe<sup>3+</sup> reduction, and are 1.6 mol m<sup>-3</sup> and 2.87 mmol m<sup>-3</sup>, respectively, for the SO<sub>4</sub><sup>2-</sup> reduction [Fumoto et al., 2008]. DNDC simulates methane production after depletions of NO<sub>3</sub><sup>-</sup>, Mn<sup>4+</sup>, Fe<sup>3+</sup>, and SO<sub>4</sub><sup>2-</sup>, when soil Eh is below -150 mV [Li et al., 2004]. Methane consumption is simulated as an oxidation reaction involving electron exchange between CH<sub>4</sub> and oxygen. In DNDC, CH<sub>4</sub> production and oxidation can occur simultaneously within a soil layer (typically 2–5 cm thick) but within relatively aerobic and anaerobic sublayers, whose volumetric fractions are determined by Eh calculations [Li, 2007].

CH<sub>4</sub> production pathways in the initial test, we modified DNDC and constrained simulations of the individual processes in CH<sub>4</sub> cycling by utilizing the field data from Stordalen.

### 3. The DNDC Model

DNDC is a process-based model developed to quantify C sequestration as well as the emissions of C and nitrogen (N) gases from terrestrial ecosystems [Li et al., 1992a, 1992b, 2000]. The model has incorporated a relatively large suite of biophysical and biogeochemical processes to compute the complex transport and transformations of C and N in terrestrial ecosystems under both aerobic and anaerobic conditions.

Redox potential, temperature, pH, and the concentrations of electron donors and acceptors are the major factors controlling the rates of  $\text{CH}_4$  production and oxidation. Methane transport from soil into atmosphere is simulated via three ways, including plant-mediated transport, ebullition, and diffusion [Fumoto *et al.*, 2008; Zhang *et al.*, 2002].

#### 4. Modifications of DNDC

In this study, we modified the version of DNDC used for simulating high-latitude soil biogeochemistry [Deng *et al.*, 2014; Zhang *et al.*, 2012]. We hypothesized that the DNDC's capacity for simulating the relative contribution of each methanogenic pathway to total  $\text{CH}_4$  production could be improved by explicitly simulating acetate dynamics, and then using acetate (instead of bulk DOC) as a substrate for acetoclastic methanogenesis. Incorporating stable C isotopic dynamics in  $\text{CH}_4$  transformations could provide a method for testing and constraining the mechanisms of  $\text{CH}_4$  cycling (production, oxidation, and transport).

##### 4.1. Modeling Acetate Dynamics and $\text{CH}_4$ Production

To explicitly simulate acetate dynamics and  $\text{CH}_4$  production pathways of AM and HM, we have introduced new processes to simulate acetate production and consumption, which jointly determine the concentration of acetate in peat soils (Figure 2). In the modified DNDC, acetate and  $\text{H}_2$  are the immediate electron donors for AM and HM, respectively, in anaerobic soils, and the rates of the reactions are controlled by the availability of acetate and  $\text{H}_2$  (Figure 2). These substrates can be produced through the mineralization of soil organic matter and anaerobic decomposition of complex dissolved organic substances. Based on Conrad [1999] and Van Bodegom and Scholten [2001], this process can be summarized as:

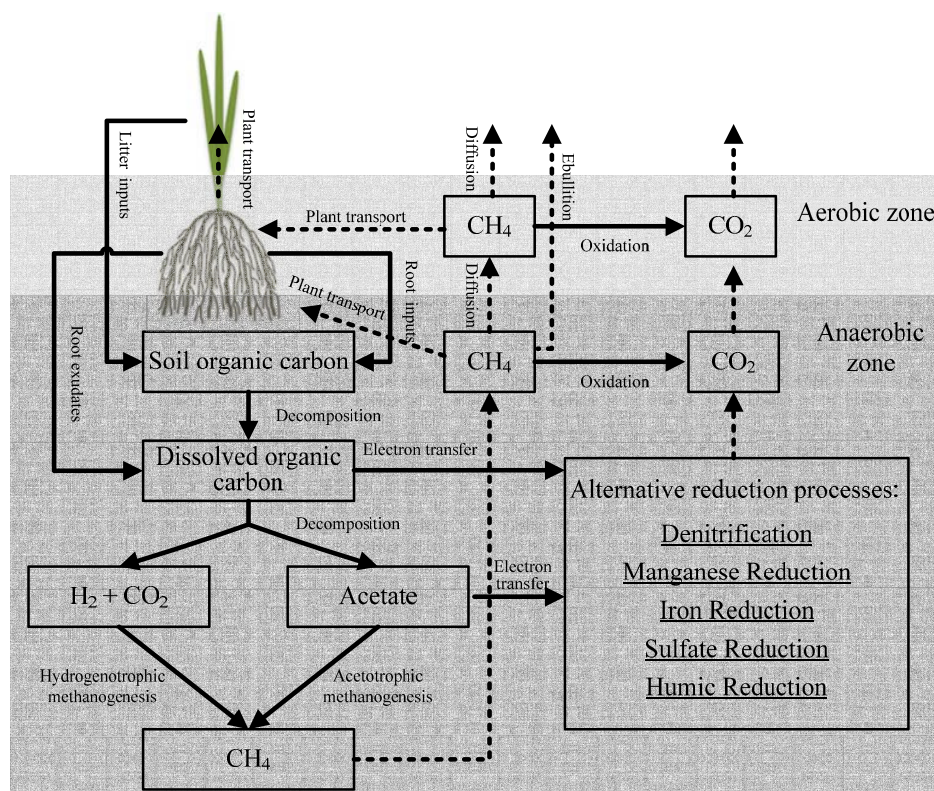
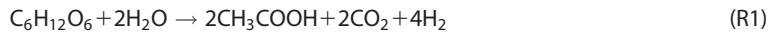


**Figure 2.** The framework for simulating soil biogeochemistry and methane dynamics in the modified DNDC. The model predicts the rate of  $\text{CH}_4$  emission by modeling  $\text{CH}_4$  production, consumption, and transport processes.  $\text{CH}_4$  production is simulated by calculating substrate concentrations (i.e., electron donors and acceptors) resulting from decomposition of SOC as well as root exudation and respiration, and then by tracking a series of reductive reactions between electron donors (i.e.,  $\text{H}_2$  and acetate) and acceptors (i.e.,  $\text{NO}_3^-$ ,  $\text{Mn}^{4+}$ ,  $\text{Fe}^{3+}$ ,  $\text{SO}_4^{2-}$ , and  $\text{CO}_2$ ) using Michaelis-Menten-based equations [Li *et al.*, 2004; Fumoto *et al.*, 2008].  $\text{CH}_4$  consumption is simulated as an oxidation reaction.  $\text{CH}_4$  transport from soil into atmosphere is simulated via three ways, plant-mediated transport, ebullition, and diffusion [Fumoto *et al.*, 2008; Zhang *et al.*, 2002].



In DNDC,  $\text{C}_6\text{H}_{12}\text{O}_6$  is represented by DOC resulting from both mineralization of SOC and plant root exudation. The reaction rate is calculated by using the Michaelis-Menten equation as follows:

$$V_{\text{AnDecom}} = V_{\text{Max\_DOC}} \cdot \frac{[\text{DOC}]}{K_{\text{AnDecom}} + [\text{DOC}]} \quad (\text{E1})$$

where,  $V_{\text{Max\_DOC}}$  is the maximum rate of anaerobic DOC decomposition, when DOC concentration is not limiting,  $[\text{DOC}]$  is the concentration of DOC ( $\text{mol m}^{-3}$ ), and  $K_{\text{AnDecom}}$  is the Michaelis half-saturation constant for this reaction.  $V_{\text{Max\_DOC}}$  is calculated by using the maximum rate of anaerobic DOC decomposition at a reference temperature ( $20^\circ\text{C}$  for this reaction) and a  $Q_{10}$  value of 2.0 for the temperature sensitivity.

Based on the stoichiometry in R1, the consumption of DOC and production of acetate,  $\text{H}_2$ , and  $\text{CO}_2$  (note that  $\text{CO}_2$  is also produced by other pathways, such as plant root respiration, AM,  $\text{CH}_4$  oxidation, and among others, in DNDC) resulting from anaerobic DOC decomposition are calculated as follows:

$$V_{\text{AnDecom}} = -\frac{d[\text{DOC}]}{dt} = 0.5 \cdot \frac{d[\text{CH}_3\text{COOH}]}{dt} = 0.5 \cdot \frac{d[\text{CO}_2]}{dt} = 0.25 \cdot \frac{d[\text{H}_2]}{dt} \quad (\text{E2})$$

Methane is primarily produced from acetotrophic and hydrogenotrophic methanogenesis for most environments, with acetate and  $\text{H}_2/\text{CO}_2$  being substrates of these two pathways, respectively [Conrad, 1989]. The reactions of acetotrophic and hydrogenotrophic methanogenesis are the following [Conrad, 1989]:



Michaelis-Menten kinetics are used for the reaction rates of the R2 and R3 [Van Bodegom and Scholten, 2001] as follows:

$$V_{\text{AM}} = V_{\text{AM\_Max}} \cdot \frac{[\text{CH}_3\text{COOH}]}{K_{\text{AM}} + [\text{CH}_3\text{COOH}]} \quad (\text{E3})$$

$$V_{\text{HM}} = V_{\text{HM\_Max}} \cdot \frac{[\text{H}_2]}{K_{\text{HM}} + [\text{H}_2]} \quad (\text{E4})$$

where,  $V_{\text{AM\_Max}}$  and  $V_{\text{HM\_Max}}$  are the maximum rates of acetotrophic and hydrogenotrophic methanogenesis, respectively, when concentrations of substrates are not limiting,  $[\text{CH}_3\text{COOH}]$  and are concentrations of acetate ( $\text{mol m}^{-3}$ ) and  $\text{H}_2$  ( $\text{mol m}^{-3}$ ), respectively, and  $K_{\text{AM}}$  and  $K_{\text{HM}}$  (Table 1) are the corresponding Michaelis half-saturation constants for these two reactions. Both  $V_{\text{AM\_Max}}$  and  $V_{\text{HM\_Max}}$  are sensitive to temperature with a  $Q_{10}$  value of 4.6 [Van Bodegom and Scholten, 2001]. Total  $\text{CH}_4$  production rate is calculated as the sum of the rates of acetate-dependent and  $\text{H}_2/\text{CO}_2$ -dependent methanogenesis.

The processes of  $\text{CH}_4$  production consume acetate,  $\text{H}_2$ , and  $\text{CO}_2$ , and produce  $\text{CO}_2$  (R2 and R3). Based on the stoichiometry in  $\text{CH}_4$  production, the consumption of acetate and production of  $\text{CO}_2$  in R2 are calculated as:

$$V_{\text{AM}} = -\frac{d[\text{CH}_3\text{COOH}]}{dt} = \frac{d[\text{CO}_2]}{dt} \quad (\text{E5})$$

The consumptions of  $\text{CO}_2$  and  $\text{H}_2$  in R3 are calculated as:

$$V_{\text{HM}} = -0.25 \cdot \frac{d[\text{H}_2]}{dt} = -\frac{d[\text{CO}_2]}{dt} \quad (\text{E6})$$

In addition to acetate consumption due to AM (R2), it has been widely observed that acetate can be consumed by other pathways, including oxidation by  $\text{O}_2$  under aerobic conditions and electron transfer between acetate and humic substances (ETAH) in anaerobic peat soils [e.g., Duddleston *et al.*, 2002; Lovley *et al.*, 1996; Segers and Kengen, 1998]. Following Segers and Kengen [1998], DNDC simulates acetate consumption due to oxidation and ETAH based on the Michaelis-Menten equation:

**Table 1.** The Model Parameters for Simulating Acetate Dynamics, Acetotrophic, Methanogenesis (AM) and Hydrogenotrophic Methanogenesis (HM), and Stable C Isotopic Dynamics at the Sphagnum and Eriophorum Sites<sup>a</sup>

Parameter	Description	Sphagnum	Eriophorum	Sources
$V_{\text{Max\_DOC}}$	Maximum anaerobic DOC decomposition rate, mol m <sup>-3</sup> d <sup>-1</sup>	0.5 • DOC	0.5 • DOC	Calibrated
$K_{\text{AnDecom}}$	Michaelis half-saturation constant for anaerobic DOC decomposition, mol m <sup>-3</sup>	1.0	1.0	Calibrated
$V_{\text{AM\_Max}}$	Maximum rate for AM, mmol kg <sup>-1</sup> dry peat d <sup>-1</sup>	0.8	4.0	Calibrated <sup>b</sup>
$K_{\text{AM}}$	Michaelis half-saturation constants for AM, mol m <sup>-3</sup>	2.56	2.56	(1)
$V_{\text{HM\_Max}}$	Maximum rate for HM, mmol kg <sup>-1</sup> dry peat d <sup>-1</sup>	7.2	4.0	Calibrated <sup>b</sup>
$K_{\text{HM}}$	Michaelis half-saturation constants for HM, mol m <sup>-3</sup>	0.0133	0.0133	(1)
$V_{\text{CAceNM\_Max}}$	Maximum rate for acetate consumption due to nonmethanogenesis pathways, mmol electron kg <sup>-1</sup> dry peat s <sup>-1</sup>	10 <sup>-2</sup>	10 <sup>-2</sup>	(2)
$K_{\text{CAceNM}}$	Michaelis half-saturation constants of acetate for acetate consumption due to nonmethanogenesis pathways, mol m <sup>-3</sup>	0.01	0.01	(2)
$K_{\text{ATEA}}$	Michaelis half-saturation constants of electron acceptors for acetate consumption due to nonmethanogenesis pathways, mol m <sup>-3</sup>	10	10	(2)
$a$	Coefficient quantifying the concentration of the electron acceptors provided by humic substances, mmol electron g <sup>-1</sup> C	2.0	1.5	Calibrated <sup>c</sup>
$\delta^{13}\text{C-DOC}$	C isotope signature of DOC	-26‰	-26‰	(3)
$\delta^{13}\text{C-CO}_2$	C isotope signature for CO <sub>2</sub> from root respiration	-26‰	-26‰	(3)
$\alpha_D$	Fractionation factor for DOC decomposition	1.000	1.000	(4)
$\alpha_{\text{AM}}$	Fractionation factor for AM	1.026	1.026	Calibrated <sup>d</sup>
$\alpha_{\text{HM}}$	Fractionation factor for HM	1.073	1.073	Calibrated <sup>d</sup>
$\alpha_{\text{MO}}$	Fractionation factor for CH <sub>4</sub> oxidation	1.025	1.025	Calibrated <sup>d</sup>
$\alpha_{\text{TP}}$	Fractionation factor for CH <sub>4</sub> emission via plant-mediated transport	1.016	1.016	Calibrated <sup>d</sup>
$\alpha_{\text{TE}}$	Fractionation factor for CH <sub>4</sub> emission via ebullition	1.000	1.000	J. Chanton (personal communication, 2015)
$\alpha_{\text{TD}}$	Fractionation factor for CH <sub>4</sub> emission via diffusion	1.001	1.001	J. Chanton (personal communication, 2015)

<sup>a</sup>References: (1) Van Bodegom and Scholten, [2001]; (2) Segers and Kengen, [1998]; (3) Corbett et al., [2013]; and (4) Conrad, [2005].

<sup>b</sup>Maximum rates for AM and HM were estimated by calibrating maximum rates of total CH<sub>4</sub> production and then distributing the calibrated value (8.0 mmol kg<sup>-1</sup> dry peat d<sup>-1</sup>) into AM and HM by referring typical relative abundance of methanogenic groups (i.e., acetotrophic groups: hydrogenotrophic groups) for different ecosystems (0.1:0.9 for Sphagnum and 0.5:0.5 for Eriophorum) [Bridgman et al., 2013].

<sup>c</sup>The coefficient,  $a$ , was estimated by constraining this parameter against the observed CH<sub>4</sub>/CO<sub>2</sub> production in the field pore-water. In 2011, the simulated ratios of CH<sub>4</sub>/CO<sub>2</sub> production at Sphagnum and Eriophorum were 0.19 and 0.40, respectively, and were close to the observed CH<sub>4</sub>/CO<sub>2</sub> production in the field pore-water sampled in June 2011 [Hodgkins et al., 2015].

<sup>d</sup> $\alpha_{\text{AM}}$ ,  $\alpha_{\text{HM}}$ ,  $\alpha_{\text{MO}}$ , and  $\alpha_{\text{TP}}$  were calibrated from their corresponding uncertainty ranges (1.000 to 1.032, 1.045 to 1.082, 1.007 to 1.031, and 1.012 to 1.021, respectively, for  $\alpha_{\text{AM}}$ ,  $\alpha_{\text{HM}}$ ,  $\alpha_{\text{MO}}$ , and  $\alpha_{\text{TP}}$ ) [Chanton et al., 1997; Conrad, 2005].

$$V_{\text{CAceNM}} = 0.125 V_{\text{CAceNM\_Max}} \cdot \frac{[\text{CH}_3\text{COOH}]}{K_{\text{CAceNM}} + [\text{CH}_3\text{COOH}]} \cdot \frac{[\text{ATEA}]}{K_{\text{ATEA}} + [\text{ATEA}]} \quad (\text{E7})$$

where,  $V_{\text{CAceNM\_Max}}$  ( $10^{-5}$  mol electron kg<sup>-1</sup> SDW (soil dry weight) s<sup>-1</sup> at a reference temperature of 15°C) is the maximum rate of consumption of acetate due to the nonmethanogenesis pathways (CAceNM),  $[\text{CH}_3\text{COOH}]$  and  $[\text{ATEA}]$  are concentrations of acetate (mol m<sup>-3</sup>) and alternative terminal electron acceptors (ATEA: O<sub>2</sub> under aerobic conditions and humic substances under anaerobic conditions in this study; mol electron m<sup>-3</sup>), respectively,  $K_{\text{CAceNM}}$  and  $K_{\text{ATEA}}$  (Table 1) are the corresponding Michaelis constants, and 0.125 is the stoichiometric constant in electron acceptor reduction (i.e., 0.125 mol acetate needed per 1.0 mol reduced electron acceptor). Similar to the R1 to R3,  $V_{\text{CAceNM\_Max}}$  is sensitive to temperature, and we use a Q<sub>10</sub> value of 2.0 to account for the influences of temperature on the reaction rate.

Because DNDC does not explicitly simulate dynamics of organic electron acceptors provided by humic substances, their concentration (mol electron m<sup>-3</sup>) is assumed to be linearly proportional to the concentration of DOC (i.e., equals to  $a \cdot [\text{DOC}]$ ) in peat soils [Heitmann et al., 2007]. Acetate consumption due to oxidation by O<sub>2</sub> occurs under aerobic conditions (e.g., in the unsaturated zone above the water table). We also use E7 to calculate the rate of this reaction, and set the  $\frac{[\text{ATEA}]}{K_{\text{ATEA}} + [\text{ATEA}]}$  term in E7 to 1.0, under the assumption that O<sub>2</sub> is not a limiting factor for this process under aerobic conditions.

In the processes of acetate oxidation by O<sub>2</sub> (under aerobic conditions) and ETAH (under anaerobic conditions), acetate is consumed and CO<sub>2</sub> is produced. Changes in acetate and CO<sub>2</sub> concentration are calculated as:

$$V_{\text{CAceNM}} = - \frac{d[\text{CH}_3\text{COOH}]}{dt} = 0.5 \cdot \frac{d[\text{CO}_2]}{dt} \quad (\text{E8})$$

With these processes, DNDC explicitly simulates acetate dynamics as well as the pathways of acetotrophic and hydrogenotrophic methanogenesis by using acetate and H<sub>2</sub>/CO<sub>2</sub> as substrates. With this

representation, acetate consumption due to the oxidation by  $O_2$  and ETAH influences the acetate concentration in soils and therefore also influences  $CH_4$  production under anaerobic conditions.

#### 4.2. Modeling Stable C Isotopic Dynamics

To enable DNDC to predict dynamics of C isotopes, i.e.,  $^{13}C$  and  $^{12}C$  transfers in the processes of  $CH_4$  production, oxidation, and transport, we have converted each of the soil C pools into two new pools (i.e.,  $^{13}C$  and  $^{12}C$  components; Figure 3) based on the principle of mass balance (E9) and  $\delta^{13}C$  values (E10) for the soil C pools:

$$M_C = M_{^{13}C} + M_{^{12}C} \quad (E9)$$

$$\delta^{13}C = \frac{M_{^{13}C}/M_{^{12}C}}{VPDB} - 1 \quad (E10)$$

where,  $M_C$ ,  $M_{^{13}C}$ , and  $M_{^{12}C}$  are masses of C,  $^{13}C$ , and  $^{12}C$  in a soil C pool, respectively;  $\delta^{13}C$  is the C isotopic signature for the corresponding soil C pool and is expressed in parts per thousand ( $\text{‰}$ ), VPDB is the standard  $\delta^{13}C$  value (i.e.,  $(^{13}C/^{12}C)_{VPDB} = 0.0112372$ ) based on the  $^{13}C$  and  $^{12}C$  abundances in the Vienna Pee Dee Belemnite international standard material.

By solving the E9 and E10, the masses of  $^{13}C$  and  $^{12}C$  in a soil C-reactant pool (e.g., DOC) can be determined by using the mass of C and  $\delta^{13}C$  value (a fixed value for initial carbon reactants, including DOC and root respiration  $CO_2$ ) as follows:

$$M_{^{12}C} = \frac{M_C}{(VPDB \cdot (1 + \delta^{13}C) + 1)} \quad (E11)$$

$$M_{^{13}C} = M_C - M_{^{12}C} \quad (E12)$$

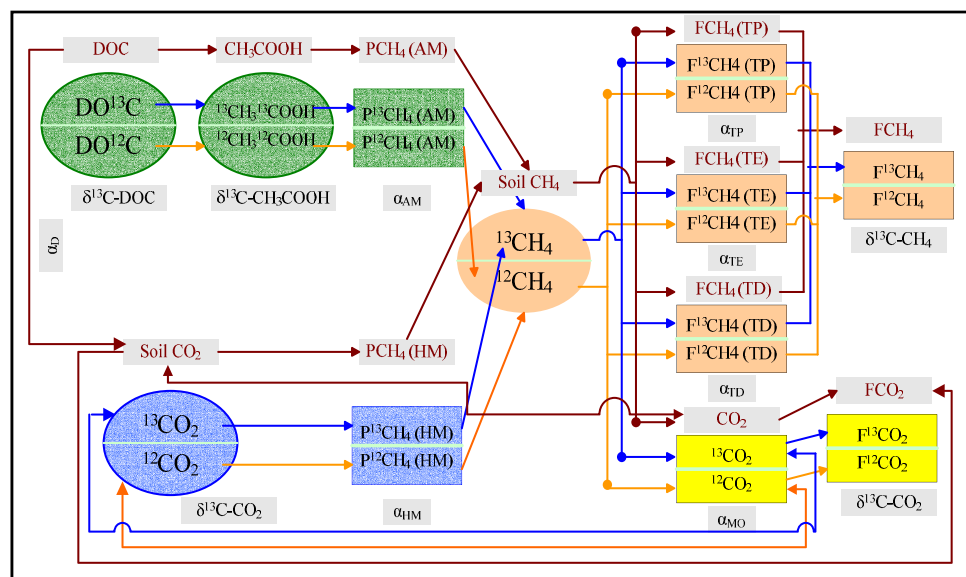


**Figure 3.** The framework for simulating stable carbon isotopic dynamics in  $CH_4$  transformations in the modified DNDC. Soil carbon pools have been converted into two new pools (i.e.,  $^{13}C$  and  $^{12}C$  components) based on the principle of mass balance and  $\delta^{13}C$  values for the soil C pools. DNDC calculates the  $^{13}C$  and  $^{12}C$  components of products by using the  $^{13}C$  and  $^{12}C$  components of reactants, simulated reaction rate, and value of isotopic fractionation factor,  $\alpha$ , for an individual process in methane transformations. The model can predict  $\delta^{13}C$  in soil  $CO_2$  and  $CH_4$  pools and emitted gas fluxes, which can be compared against observations from field studies or laboratory experiments for further testing and constraining simulations of the individual processes in  $CH_4$  biogeochemistry. The abbreviations D, AM, HM, and MO indicate the processes of DOC decomposition, acetotrophic methanogenesis, hydrogenotrophic methanogenesis, and methane oxidation, respectively. Fluxes of  $CH_4$  ( $FCH_4$ ) are transported through plant (TP), ebullition (TE), and diffusion (TD). The processes of acetate consumptions due to the  $O_2$  reduction and electron transfer between acetate and humic substances are not shown for the reason of clarity, and the  $^{13}C$  and  $^{12}C$  components of soil acetate and  $CO_2$  pools are not changed by these processes because the fractionation factor,  $\alpha$ , for them are 1.0 [Conrad, 2005; Corbett et al., 2013].

Isotopic fractionation in biogeochemical reactions (e.g., CH<sub>4</sub> production and oxidation) can be quantified by using a fractionation factor,  $\alpha$ , defined as [Hayes, 1993]:

$$\alpha = \frac{(^{13}\text{C}/^{12}\text{C})_{\text{Reactant}}}{(^{13}\text{C}/^{12}\text{C})_{\text{Product}}} \quad (\text{E13})$$

The value of  $\alpha$  can be determined by measuring the abundances of <sup>13</sup>C and <sup>12</sup>C in laboratory experiments. The sum of the produced <sup>13</sup>C and <sup>12</sup>C components equals the total C product based on the mass balance principle:

$$P_C = P_{^{13}\text{C}} + P_{^{12}\text{C}} \quad (\text{E14})$$

where,  $P_C$ ,  $P_{^{13}\text{C}}$ , and  $P_{^{12}\text{C}}$  are masses of C, <sup>13</sup>C, and <sup>12</sup>C, respectively, of total produced C in a C-producing reaction (e.g., the produced C-CH<sub>3</sub>COOH equals to the sum of the produced <sup>13</sup>C-CH<sub>3</sub>COOH and <sup>12</sup>C-CH<sub>3</sub>COOH for the R1).

By solving E13 and E14, the masses of <sup>13</sup>C and <sup>12</sup>C in a C product (e.g., CH<sub>3</sub>COOH) can be calculated by using the <sup>13</sup>C and <sup>12</sup>C contents in the corresponding C precursors (e.g., DOC for the acetate production), fractionation factor ( $\alpha$ ), and rate of the corresponding reaction (a variable simulated by DNDC) as follows:

$$P_{^{12}\text{C}} = \frac{P_C}{((^{13}\text{C}/^{12}\text{C})_{\text{Reactant}}/\alpha + 1)} \quad (\text{E15})$$

$$P_{^{13}\text{C}} = P_C - P_{^{12}\text{C}} \quad (\text{E16})$$

The principles of mass balance and C isotopic fractionation are applied to all processes in CH<sub>4</sub>cycling (Figure 3), although the fractionation factor ( $\alpha$ ) may be close or equal to 1.0 (i.e., no isotopic fractionation effect) for some processes (e.g., anaerobic DOC decomposition and acetate consumptions due to the O<sub>2</sub> reduction and EТАH pathways) [Conrad, 2005; Corbett *et al.*, 2013]. For each process, the <sup>13</sup>C and <sup>12</sup>C components of products can be calculated by using the <sup>13</sup>C and <sup>12</sup>C components of reactants, reaction rate (simulated by DNDC), and isotopic fractionation factor ( $\alpha$ ). To predict the  $\delta^{13}\text{C}$  of CH<sub>4</sub> fluxes, DNDC calculates: (1) the <sup>13</sup>C and <sup>12</sup>C components in DOC pool, (2) the <sup>13</sup>C and <sup>12</sup>C components in pools of C substrates (i.e., acetate and CO<sub>2</sub>) for CH<sub>4</sub> production, (3) production of acetate-induced <sup>13</sup>CH<sub>4</sub> and <sup>12</sup>CH<sub>4</sub>, (4) production of H<sub>2</sub>/CO<sub>2</sub>-induced <sup>13</sup>CH<sub>4</sub> and <sup>12</sup>CH<sub>4</sub>, (5) <sup>13</sup>C and <sup>12</sup>C components in soil CH<sub>4</sub> and CO<sub>2</sub> pools by considering isotopic fractionation in the processes of CH<sub>4</sub> production and consumption, (6) <sup>13</sup>CH<sub>4</sub> and <sup>12</sup>CH<sub>4</sub> fluxes through each transport pathway (i.e., plant-mediated transport, ebullition, and diffusion) by considering isotopic fractionation in the processes of CH<sub>4</sub> transport, (7)  $\delta^{13}\text{C}$  of emitted gas fluxes, and (8) <sup>13</sup>C and <sup>12</sup>C components in remaining dissolved CH<sub>4</sub> and CO<sub>2</sub> pools (Figure 3). It should be noted that DNDC simulates CH<sub>4</sub> production after depletions of NO<sub>3</sub><sup>-</sup>, Mn<sup>4+</sup>, Fe<sup>3+</sup>, and SO<sub>4</sub><sup>2-</sup> and assumes that these nonmethanogenic reductions do not affect the  $\delta^{13}\text{C}$  value of the acetate for CH<sub>4</sub> production.

After incorporating the stable C isotopic dynamics into the DNDC's framework, the model can predict  $\delta^{13}\text{C}$  in soil CO<sub>2</sub> and CH<sub>4</sub> pools and emitted gas flux. These outputs can be compared against observations from field studies or laboratory experiments for further testing and constraining simulations of the individual processes in CH<sub>4</sub> cycling.

## 5. Model Evaluation

We conducted model comparisons against observed data sets for two sites at Stordalen Mire, a moss-dominated site with degrading permafrost (active layer of about 1.2 m), and a wetter sedge-dominated site with no detectable underlying permafrost [McCalley *et al.*, 2014]. The sites are referred to as Sphagnum and Eriophorum based on their dominant vegetation cover. Simulations of CH<sub>4</sub> fluxes, the relative contributions of the two CH<sub>4</sub> production pathways to the total production inferred from relative abundance of different methanogen functional groups, and C isotopic composition of CH<sub>4</sub> fluxes were compared to field data (see section 2). Simulations were run for both sites from 2010 to 2013, using daily meteorological data (i.e., maximum, mean, and minimum air temperature, precipitation, solar radiation, wind speed, and humidity) recorded at ANS (Figure 1). Simulated soil climate conditions were initialized by repeating the climate data in 2010 until the simulated annual mean soil temperature was stable. Then the vegetation and soil

biogeochemical modules were activated and the model was run for 2011 (calibration) and continuously from 2011 to 2013, with 2012 and 2013 for validation. Most input parameters (soils, hydrology, and vegetation) were set to the values used in previous simulations performed for the same sites [Deng *et al.*, 2014]. In order to reduce the influence of WTD prediction-error on soil thermal and biogeochemical processes, we used the observed WTDs to drive the model if the measurements were available; if daily WTD data were not available, we interpolated daily values between observations as in Deng *et al.* [2014], using the hydrological parameters developed in that study. Based on new data from the Stordalen sites, pH ( $\text{H}_2\text{O}$ ) was set to 4.2 and 5.7, and peat C/N ratios were set to 60 and 30 for the Sphagnum and Eriophorum sites, respectively [Hodgkins *et al.*, 2014].

Several new model parameters are needed to simulate acetate dynamics, methanogenesis, and stable carbon isotope fractionation (see equations (1), (3), (4), (7), (15), and (16); Figure 3). Parameters were set either to literature values or calibrated against field observations of  $\text{CH}_4$  fluxes and  $\delta^{13}\text{C}-\text{CH}_4$  in 2011 (Table 1). The calibrated parameters included maximum rate ( $V_{\text{Max\_DOC}}$ ) and half-saturation constant ( $K_{\text{AnDecom}}$ ) for anaerobic DOC decomposition, maximum rates for AM ( $V_{\text{AM\_Max}}$ ) and HM ( $V_{\text{HM\_Max}}$ ), the coefficient quantifying the concentration of the electron acceptors provided by humic substances (a), and fractionation factors for AM ( $\alpha_{\text{AM}}$ ), HM ( $\alpha_{\text{HM}}$ ),  $\text{CH}_4$  oxidation ( $\alpha_{\text{MO}}$ ), and plant-mediated  $\text{CH}_4$  transport ( $\alpha_{\text{TP}}$ ).  $V_{\text{Max\_DOC}}$  and  $K_{\text{AnDecom}}$  were estimated by calibrating the simulated  $\text{CH}_4$  fluxes with the observed  $\text{CH}_4$  fluxes in 2011. The ratio of  $V_{\text{AM\_Max}}:V_{\text{HM\_Max}}$  was fixed by referring typical relative abundance of methanogenic groups (i.e., acetotrophic groups:hydrogenotrophic groups) for different ecosystems (0.1:0.9 for Sphagnum and 0.5:0.5 for Eriophorum) [Bridgham *et al.*, 2013]. Maximum rates for AM and HM were then estimated by calibrating maximum rates of total  $\text{CH}_4$  production with the observed  $\text{CH}_4$  fluxes in 2011 and then distributing the calibrated value ( $8.0 \text{ mmol kg}^{-1} \text{ dry peat d}^{-1}$ ) into AM and HM using the ratios of  $V_{\text{AM\_Max}}:V_{\text{HM\_Max}}$ . The coefficient, a, was estimated as 2.0 and 1.5 for the Sphagnum and Eriophorum sites, respectively, by constraining the parameter against the observed  $\text{CH}_4/\text{CO}_2$  production in the field pore-water. The simulated production ratios of  $\text{CH}_4/\text{CO}_2$  at the Sphagnum and Eriophorum sites were 0.19 and 0.40, respectively, in 2011, and were close to the observed  $\text{CH}_4/\text{CO}_2$  production in the field pore-water sampled in June 2011 [Hodgkins *et al.*, 2015]. The fractionation factors,  $\alpha_{\text{AM}}$ ,  $\alpha_{\text{HM}}$ ,  $\alpha_{\text{MO}}$ , and  $\alpha_{\text{TP}}$ , were estimated by calibrating the simulated  $\delta^{13}\text{C}-\text{CH}_4$  with the observed  $\delta^{13}\text{C}-\text{CH}_4$  in 2011 after fixing  $V_{\text{Max\_DOC}}$ ,  $K_{\text{AnDecom}}$ ,  $V_{\text{AM\_Max}}$ ,  $V_{\text{HM\_Max}}$ , and a. The reported ranges of  $\alpha_{\text{AM}}$ ,  $\alpha_{\text{HM}}$ ,  $\alpha_{\text{MO}}$ , and  $\alpha_{\text{TP}}$  were 1.000–1.032, 1.045–1.082, 1.007–1.031, and 1.012–1.021, respectively [Chanton *et al.*, 1997; Conrad, 2005]. Through calibration with the  $\delta^{13}\text{C}-\text{CH}_4$  observations in 2011, the values of  $\alpha_{\text{AM}}$ ,  $\alpha_{\text{HM}}$ ,  $\alpha_{\text{MO}}$ , and  $\alpha_{\text{TP}}$  were set as 1.026, 1.073, 1.025, and 1.016, respectively. In general, the input parameters described above were primarily determined by calibrating against the field data of  $\text{CH}_4$  fluxes and  $\delta^{13}\text{C}-\text{CH}_4$  in 2011, and the calibrated model was then validated by comparing simulations against observations of  $\text{CH}_4$  fluxes and  $\delta^{13}\text{C}-\text{CH}_4$  in 2012 and 2013, as well as estimates of the relative contribution of the two  $\text{CH}_4$  production pathways.

### 5.1. Methane Fluxes

Simulated seasonal patterns of  $\text{CH}_4$  fluxes were close to the observed fluxes for both the calibration (2011) and validation (2012 and 2013) periods at the Sphagnum site. High peaks were noted in summer seasons from July to September in both the simulations and field records (Figure 4). In addition, DNDC simulated fluctuations of  $\text{CH}_4$  fluxes resulting from water table fluctuations (between –25 and 0 cm) at this site, consistent with observations (Figures 4a–4c). Correlation (R) values of model to field data were 0.86 and 0.61 in 2012 and 2013, respectively, indicating that the simulated seasonal variation of daily  $\text{CH}_4$  fluxes was significantly correlated with the corresponding observations in each year ( $p < 0.001$ ). The simulated cumulative  $\text{CH}_4$  fluxes in 2012 and 2013 were 2.43 and 2.89 g  $\text{CH}_4\text{-C m}^{-2}$ , respectively, comparable with the corresponding observations of 2.91 and 2.45 g  $\text{CH}_4\text{-C m}^{-2}$  with the root mean square errors (RMSE) calculated as 0.48 and 0.44 g  $\text{CH}_4\text{-C m}^{-2}$ , respectively, in 2012 and 2013 (Table 2). The relative root mean square errors (RRMSE) between the simulated and observed cumulative  $\text{CH}_4$  fluxes in 2012 and 2013 were 16% and 18%, respectively, which were less than the standard deviations of the observations in each year, meaning that the discrepancies between the model and field data were within the natural variation of the field observations.

At the Eriophorum site, the simulated seasonal patterns of  $\text{CH}_4$  fluxes by the modified DNDC were comparable with the observations (Figures 4d–4f); with R values of 0.86 and 0.68 in 2012 and 2013 ( $p < 0.001$ ), respectively. However, simulated fluxes were higher than observations during the early growing season in

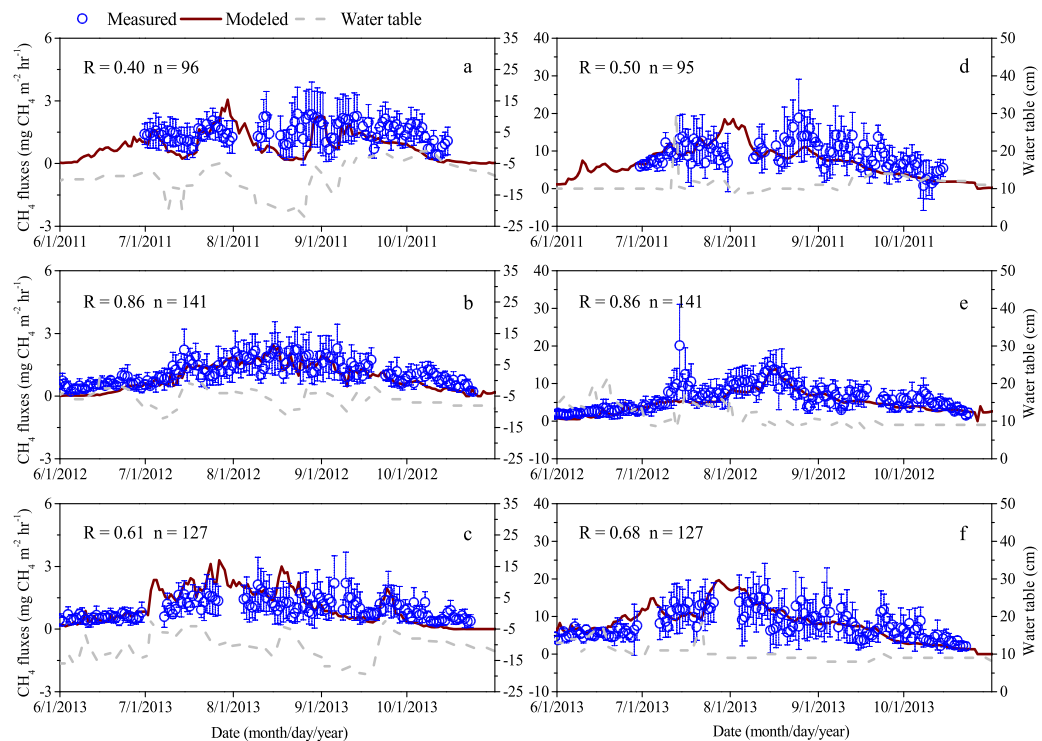


**Figure 4.** Water table dynamics (positive values for above-ground and negative values for below-ground), simulated, and observed daily  $\text{CH}_4$  fluxes at the (a–c) Sphagnum and (d–f) Eriophorum sites during 2011–2013 growing seasons. Note the difference in  $\text{CH}_4$  flux and water table scales between (left) Sphagnum and (right) Eriophorum plots. The correlations between the simulated and observed daily  $\text{CH}_4$  fluxes were significant for all cases ( $p < 0.001$ ). The observed  $\text{CH}_4$  fluxes are the means of three (Sphagnum) or two (Eriophorum) chamber replicates and vertical bars are standard deviations of the replicate daily means.

2013 (Figure 4f). Daily  $\text{CH}_4$  fluxes at the Eriophorum site were generally higher than that at Sphagnum. The observed cumulative  $\text{CH}_4$  fluxes were 15.71 and 19.57  $\text{g CH}_4\text{-C m}^{-2}$  in 2012 and 2013, respectively, while the corresponding simulations were 14.38 and 22.72  $\text{g CH}_4\text{-C m}^{-2}$ . The RMSE values were 1.33 and 3.15  $\text{g CH}_4\text{-C m}^{-2}$ , respectively, for 2012 and 2013, and the corresponding RRMSE values were 8% and 16%, respectively (Table 2). Discrepancies between the simulations and observations were close to or less than the standard deviations of the observed cumulative  $\text{CH}_4$  fluxes.

### 5.2. $\text{CH}_4$ Production Pathways

Simulated seasonal patterns for the HM and AM were similar in each year at Sphagnum, with relative high rates in summer (July–September) and reductions in the production rates following drops in the water table (Figures 5a–5c). HM was the primary  $\text{CH}_4$  production pathway at the Sphagnum site, contributing

**Table 2.** Comparison of the Modeled (M) and Observed (O)  $\text{CH}_4$  Fluxes (in  $\text{g CH}_4\text{-C m}^{-2}$ ) During Three Study Periods at the Sphagnum and Eriophorum Sites<sup>a</sup>

Year	O <sup>b</sup>	Sphagnum			Eriophorum			
		M	RMSE <sup>c</sup>	RRMSE <sup>c</sup>	O	M	RMSE	RRMSE
2011	2.87[1.27]	2.00	0.87	30	17.17[1.81]	16.35	0.82	5
2012	2.91[0.93]	2.43	0.48	16	15.71[0.64]	14.38	1.33	8
2013	2.45[0.69]	2.89	0.44	18	19.57[3.93]	22.72	3.15	16

<sup>a</sup>The study period is the span during which continuous measurements of daily  $\text{CH}_4$  fluxes were available. To calculate the total  $\text{CH}_4$  emissions over the sampling period in each year, fluxes for the days lacking measurements were determined using the arithmetic mean fluxes of the two closest days when observations were performed. Daily fluxes from either direct measurements or gap-filling were then summed up to calculate the growing period cumulative  $\text{CH}_4$  emissions.

<sup>b</sup>Each figure number within the bracket is the standard deviation of three (Sphagnum) or two (Eriophorum) replicate auto chamber plots.

<sup>c</sup>RMSE and RRMSE are root mean squared error ( $\text{g CH}_4\text{-C m}^{-2}$ ) and relative root mean squared error (%), respectively.

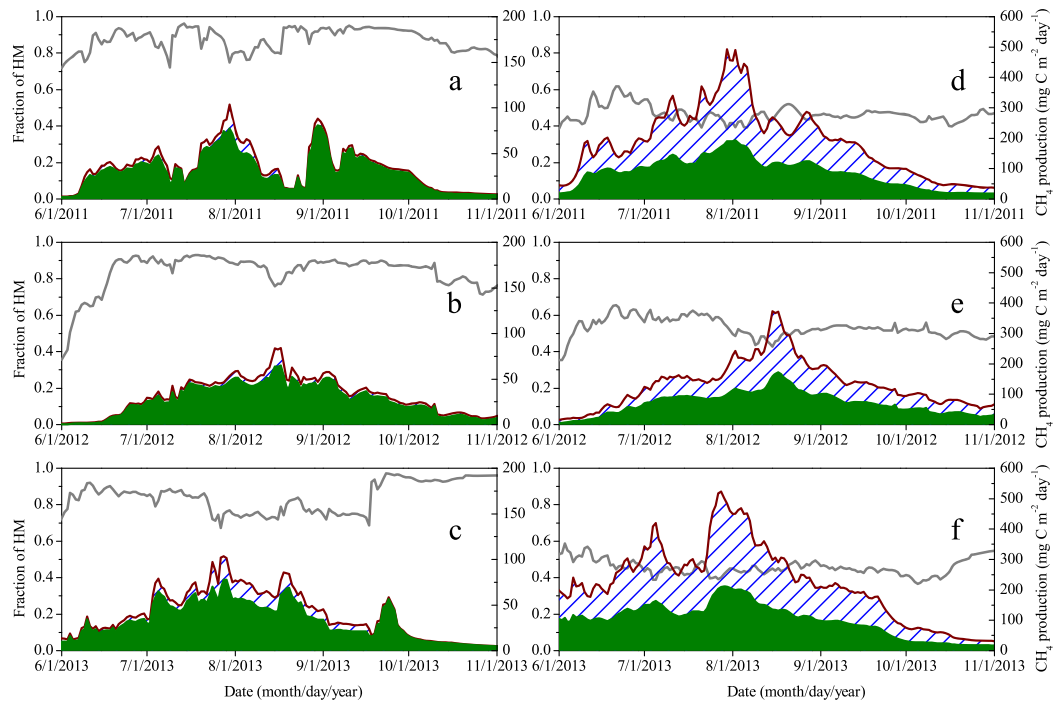


**Figure 5.** Simulated daily  $\text{CH}_4$  production (brown line;  $\text{mg } \text{CH}_4\text{-C m}^{-2} \text{ d}^{-1}$ ) at the (a–c) Sphagnum and (d–f) Eriophorum sites during 2011–2013, and its partitioning into hydrogenotrophic methanogenesis (HM, green shading) and acetotrophic methanogenesis (AM, blue diagonal lines), respectively. The grey lines represent the fractional contribution of HM to total  $\text{CH}_4$  production.

85% on average to the production (range = 36%–97%) over the three seasons from 2011 to 2013. We compared the simulated relative contribution of methanogenic pathways to total  $\text{CH}_4$  production against the observations of relative abundance of methanogen functional groups on individual days in 2011 (Table 3). The 10 day averages of the simulated contribution for hydrogenotrophic pathway through the growing season were 90%, 92%, 91%, and 82%, respectively, following 15 June, 12 July, 15 August, and 15 October. The simulations of the modified DNDC improved upon the results predicted by an early version without the aforementioned modifications [Deng et al., 2014], and were comparable with the corresponding observations of 90%, 85%, 94%, and 85%, respectively (Table 3; note that the AM fraction equals 1.0 minus the HM fraction).

At the Eriophorum site, simulated high peaks of methanogenesis occurred from July to September, with the AM and HM pathways contributed approximately equally to total methanogenesis during the growing seasons (Figures 5d–5f). The average contributions of hydrogenotrophic and acetotrophic pathways to total  $\text{CH}_4$  production were calculated as 51% (range: 35%–61%) and 49% (range: 39%–65%), respectively, across

**Table 3.** Modeled (M) and Observed (O) Relative Fractional Contribution of the Hydrogenotrophic Methanogenic Pathway (HM) to Total  $\text{CH}_4$  Production at the Stordalen Sphagnum and Eriophorum Sites on Individual Days in 2011<sup>a</sup>

Date	Sphagnum			Eriophorum		
	O <sup>b</sup>	M <sub>M</sub> <sup>c</sup>	M <sub>O</sub> <sup>c</sup>	O	M <sub>M</sub>	M <sub>O</sub>
15 Jun	0.90	0.90	0.44	0.68	0.53	0.45
12 Jul	0.85	0.92	0.46	0.61	0.49	0.40
16 Aug	0.94	0.91	0.40	0.59	0.49	0.42
16 Oct	0.85	0.82	0.59	0.54	0.58	0.51

<sup>a</sup>The acetoclastic methanogenic pathway (AM) fraction equals 1.0 minus this fraction.

<sup>b</sup>Observed production pathway partitioning was inferred from the relative abundance of methanogen functional groups [McCalley et al., 2014].

<sup>c</sup>Modeled results are 10 day averages of contribution of hydrogenotrophic and acetotrophic pathways following the corresponding date with observation, and were produced with the modified ( $M_M$ ) and an older ( $M_O$ ) version of DNDC. The old version in Deng et al. [2014] did not explicitly simulate acetate dynamics and used DOC as a substrate for acetoclastic methanogenesis.

the three seasons from 2011 to 2013. The 10 days averages of the simulated contributions for HM were 53%, 49%, 49%, and 58%, respectively, following 15 June, 12 July, 15 August, and 15 October in 2011. The simulations by the modified DNDC improved upon the results from an early version without modifications, and were comparable with the corresponding observations, which were 68%, 61%, 59%, and 54%, respectively (Table 3; note that the AM fraction equals 1.0 minus the HM fraction).

### 5.3. CH<sub>4</sub> Flux Isotopic Composition

Unlike the flux rates, no clear seasonal pattern appeared for  $\delta^{13}\text{C-CH}_4$  at either the Sphagnum or Eriophorum sites. And there is no correlation between the  $\delta^{13}\text{C-CH}_4$  and flux rates. However, both the simulations and observations showed a consistent divergence of around 8‰ between these two sites during both the calibration (2011) and validation (2012 and 2013) periods although the divergence was occasionally overlain by fluctuations of  $\delta^{13}\text{C-CH}_4$ , likely due to seasonal fluctuations in the rates of CH<sub>4</sub> production, oxidation, and transport (Figure 6).

The means of the observed  $\delta^{13}\text{C-CH}_4$  at the Sphagnum and Eriophorum sites were  $-79\text{\textperthousand}$  and  $-67\text{\textperthousand}$ , respectively, for the calibration year 2011. For the validation periods in 2012 and 2013, the means of the observed  $\delta^{13}\text{C-CH}_4$  at Sphagnum and Eriophorum were  $-71\text{\textperthousand}$  and  $-65\text{\textperthousand}$ , respectively. The DNDC simulated corresponding  $\delta^{13}\text{C-CH}_4$  at the Sphagnum and Eriophorum sites were  $-76\text{\textperthousand}$  and  $-67\text{\textperthousand}$  (2011) and  $-71\text{\textperthousand}$  and  $-66\text{\textperthousand}$  (2012 and 2013), respectively. Both the simulations and observations showed that most of the  $\delta^{13}\text{C-CH}_4$  values distributed below  $-65\text{\textperthousand}$  for Sphagnum and between  $-70\text{\textperthousand}$  and  $-60\text{\textperthousand}$  for Eriophorum (Figure 7). The simulations by the modified DNDC improved upon the predictions by the version without acetate dynamics, which failed to capture the observed relative contribution of methanogenic pathways to total CH<sub>4</sub> production (Table 3) and thereafter predicted  $\delta^{13}\text{C-CH}_4$  with systematic discrepancies in comparison with the field records (Table 4).

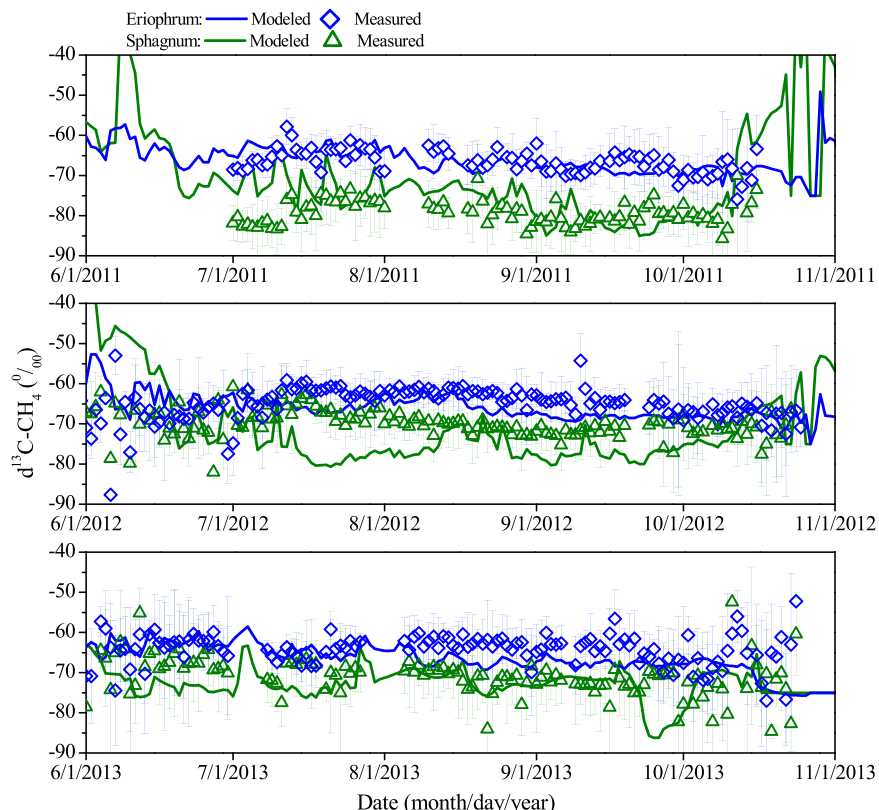


**Figure 6.** Simulated and observed  $\delta^{13}\text{C}$  of daily CH<sub>4</sub> fluxes at the Sphagnum and Eriophorum sites during 2011–2013. The observed  $\delta^{13}\text{C}$  values are the means of three (Sphagnum) or two (Eriophorum) chamber replicates and vertical bars are standard deviations of the replicates [McCalley *et al.*, 2014].

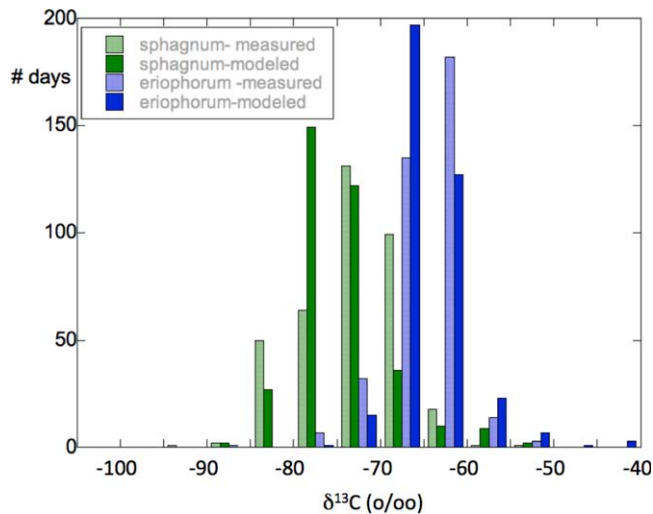


**Figure 7.** Simulated and observed distribution of  $\delta^{13}\text{C}$  (in ‰) of daily  $\text{CH}_4$  fluxes at the Stordalen Sphagnum (green) and Eriophorum (blue) sites for all days in 2011–2013 with chamber data ( $n \sim 370$  days) binned in 5‰ intervals (bars). Simulations were produced with the modified DNDC. Both the field observations and simulations showed that most of the  $\delta^{13}\text{C}$  values distributed below  $-65\text{‰}$  for Sphagnum and between  $-70\text{‰}$  and  $-60\text{‰}$  for Eriophorum.

[Chanton *et al.*, 1997; Conrad, 2005; Ehleringer *et al.*, 2000]. Mean simulated  $\delta^{13}\text{C-CH}_4$  from 1 June to 31 October 2013 under each of the scenarios were compared with a sensitivity index (SI) [Nearing *et al.*, 1990] calculated as follows:

$$SI = ((O_2 - O_1) / O_{avg}) / ((I_2 - I_1) / I_{avg}) \quad (\text{E17})$$

where  $I_1$ ,  $I_2$ , and  $I_{avg}$  are the minimum, maximum, and average values of a selected input parameter,  $O_1$ ,  $O_2$ , and  $O_{avg}$  are the corresponding modeled  $\delta^{13}\text{C-CH}_4$ .

The sensitivity results (Table 5) indicate that (1)  $\delta^{13}\text{C}$  in emitted  $\text{CH}_4$  was very sensitive to variation in  $\alpha_{AM}$ ,  $\alpha_{HM}$ , and  $\alpha_{MO}$  with more enriched  $\delta^{13}\text{C}$  resulting from smaller fractionation effects in  $\text{CH}_4$  production ( $\alpha_{AM}$  and  $\alpha_{HM}$ ) and larger fractionation effects in  $\text{CH}_4$  oxidation ( $\alpha_{MO}$ ), and (2) the variation in transport fractionation ( $\alpha_{TP}$ ) exerted a moderate influence on  $\delta^{13}\text{C-CH}_4$  as compared to other factors, and larger fractionation effects in  $\text{CH}_4$  transport resulted in smaller  $\delta^{13}\text{C-CH}_4$  (i.e., more depleted  $^{13}\text{C}$ ) for the test case.

## 7. Discussion

Considering microbial communities when developing ecosystem models is an important next step toward accurately simulating ecosystem processes and predicting responses to environmental change [Wieder *et al.*, 2013; Graham *et al.*, 2012, 2014]. For example, recent research at Stordalen Mire has highlighted the need to consider microbial ecology and its impact on  $\text{CH}_4$  production and isotopes when modeling the  $\text{CH}_4$  emissions from thawing permafrost [McCalley *et al.*, 2014]. The challenge is how to model shifts in microbial

## 6. Sensitivity Analysis

To investigate the general behaviors of the modified DNDC in predicting C isotopic signature in  $\text{CH}_4$  fluxes, we conducted a sensitivity analysis by varying several input parameters that have an uncertainty range, including the C isotopic signatures for DOC ( $\delta^{13}\text{C-DOC}$ ) and root respiration  $\text{CO}_2$  ( $\delta^{13}\text{C-CO}_2\text{-root}$ ), and fractionation factors for the processes of  $\text{CH}_4$  production ( $\alpha_{AM}$  and  $\alpha_{HM}$ ),  $\text{CH}_4$  oxidation ( $\alpha_{MO}$ ), and plant-mediated  $\text{CH}_4$  transport ( $\alpha_{TP}$ ). The baseline scenario was set based on the actual conditions at Eriophorum, and alternative scenarios were created by varying a single input parameter while keeping others constant. The varied ranges were  $-30\text{‰}$  to  $-22\text{‰}$  for  $\delta^{13}\text{C-DOC}$  and  $\delta^{13}\text{C-CO}_2\text{-root}$ , 1.000–1.032 for  $\alpha_{AM}$ , 1.045–1.082 for  $\alpha_{HM}$ , 1.007–1.031 for  $\alpha_{MO}$ , and 1.012–1.021 for  $\alpha_{TP}$ .

**Table 4.** Modeled (M) and Observed (O)  $\delta^{13}\text{C}$  of Daily  $\text{CH}_4$  Fluxes at the Sphagnum and Eriophorum Sites

Period	Sphagnum			Eriophorum		
	O <sup>a</sup>	M <sub>M</sub> <sup>b</sup>	M <sub>O</sub> <sup>b</sup>	O	M <sub>M</sub>	M <sub>O</sub>
2011	-79 [-86 – -70]	-76 [-85 – -55]	-62 [-72 – -47]	-67 [-76 – -58]	-67 [-73 – -61]	-64 [-69 – -58]
2012–2013	-71 [-94 – -52]	-71 [-86 – -40]	-59 [-75 – -20]	-65 [-88 – -52]	-66 [-76 – -40]	-63 [-74 – -37]

<sup>a</sup>Data and numbers in the bracket are the means and ranges of  $\delta^{13}\text{C-CH}_4$ , respectively, across all days with chamber data.

<sup>b</sup>Simulations were produced with the modified (M<sub>M</sub>) and an older (M<sub>O</sub>) version of DNDC. The old version in Deng *et al.* [2014] did not explicitly simulate acetate dynamics and used DOC as a substrate for acetoclastic methanogenesis.

**Table 5.** Calculated Sensitivity Indices Quantifying the Impacts of Variations in C Isotopic Signature of Substrates (DOC and Root Respired CO<sub>2</sub>) and Fractionation Factors<sup>a</sup> on δ<sup>13</sup>C-CH<sub>4</sub> Predicted by the Modified DNDC

Items	δ <sup>13</sup> C-DOC	δ <sup>13</sup> C-CO <sub>2</sub>	α <sub>AM</sub>	α <sub>HM</sub>	α <sub>MO</sub>	α <sub>TP</sub>
Average	-26‰	-26‰	1.016	1.064	1.019	1.017
Minimum	-30‰	-30‰	1.000	1.045	1.007	1.012
Maximum	-22‰	-22‰	1.032	1.082	1.031	1.021
SI <sup>b</sup>	0.21	0.15	8.82	6.85	-5.58	2.82

<sup>a</sup>α<sub>AM</sub>, α<sub>HM</sub>, α<sub>MO</sub>, and α<sub>TP</sub> are fractionation factors for the processes of acetotrophic methanogenesis, hydrogenotrophic methanogenesis, CH<sub>4</sub> oxidation, and plant-mediated CH<sub>4</sub> transport, respectively. The uncertainty ranges of δ<sup>13</sup>C-DOC, δ<sup>13</sup>C-CO<sub>2</sub>, α<sub>AM</sub>, α<sub>HM</sub>, α<sub>MO</sub>, and α<sub>TP</sub> were determined from Chanton et al. [1997], Conrad [2005], and Ehleringer et al. [2000].

<sup>b</sup>SI is a relative sensitivity index, the higher the absolute value of the SI, the greater the impact the input has on the output.

metabolism and the resulting change in CH<sub>4</sub> emissions and δ<sup>13</sup>C-CH<sub>4</sub> across spatially complex, thawing northern peatlands. Incorporating stable isotopic dynamics into traditional biogeochemical models is at an early stage. There are no other CH<sub>4</sub> models that can simulate stable carbon isotopic dynamics [Xu et al., 2016].

In this study, we used microbial and isotopic field data to identify a shortcoming in DNDC simulations of CH<sub>4</sub> production pathways in wetland sites. The initial disconnect between DNDC outputs and field measurements of CH<sub>4</sub> production pathway, despite reasonable CH<sub>4</sub> flux simulations [Deng et al., 2014] and incorporation of both AM and HM pathways [Fumoto et al., 2008] was primarily due to using bulk DOC as a substrate for acetoclastic methanogenesis. The disconnect exemplifies how models can get the correct net CH<sub>4</sub> emission, while missing or misrepresenting key underlying mechanisms. Consideration of isotopic and microbial prevalence data led to the addition of an explicit acetate metabolism pathway providing the substrate for acetotrophic methanogenesis, which appreciably improved DNDC's simulation of the relative contributions of AM and HM pathways to total CH<sub>4</sub> emission (Figure 8). Further, incorporation of stable C isotope dynamics into DNDC now provides an additional internal metric for testing and constraining the

processes (production, oxidation, transport) that underlie CH<sub>4</sub> fluxes in DNDC. We note that adding the new processes also introduced new parameters that are not well-enough constrained by literature values and required calibration.

We also modified DNDC by explicitly simulating acetate dynamics and pathways of acetotrophic and hydrogenotrophic methanogenesis, which we hypothesized could improve DNDC's simulation of the relative contribution of methanogenic pathways to total CH<sub>4</sub> production. Model tests against field measurements indicated that the modified DNDC successfully captured the differences between the Sphagnum and Eriophorum sites in total CH<sub>4</sub> fluxes, relative contribution of methanogenic pathways to CH<sub>4</sub> production, and the δ<sup>13</sup>C isotopic signature of emitted CH<sub>4</sub> (Figure 8). In earlier analyses, we found that CH<sub>4</sub> flux differences between the Sphagnum and Eriophorum sites were a result of site differences in soil environments and vegetation characteristics [Deng et al., 2014]. The simulated different

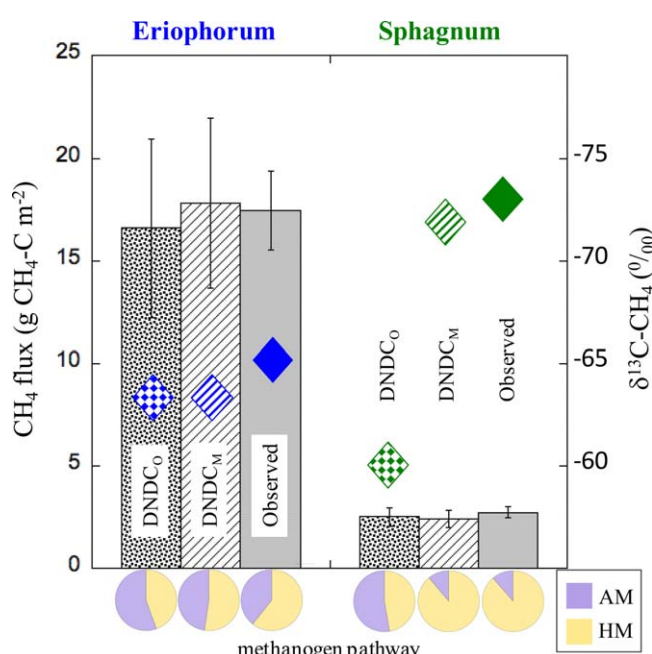


**Figure 8.** Mean CH<sub>4</sub> flux (bars with interannual standard deviation, left axis) and δ<sup>13</sup>C of emitted methane (diamonds, right axis) during three study periods from 2011 to 2013, and 2011 relative contribution of hydrogenotrophic and acetotrophic methane production pathways (pie charts, observed inferred from the relative abundance of methanogen functional groups) [McCalley et al., 2014] at the Eriophorum and Sphagnum sites. Comparison across an older DNDC (DNDC<sub>O</sub>) version [Deng et al., 2014], the modified DNDC (DNDC<sub>M</sub>), and field observations at Stordalen mire in Sweden.

contribution of methanogenic pathways could be primarily attributed to different vegetation characteristics between these two sites. Based on E3 and E4, the relative contribution of methanogenic pathways to total CH<sub>4</sub> production is jointly controlled by the ratio of  $V_{AM\_Max}:V_{HM\_Max}$  and substrate concentration, which were either based on vegetation types (Table 1) or simulated by tracking substrate production and consumption closely related to vegetation characteristics. The differences in CH<sub>4</sub> metabolism between the Sphagnum and Eriophorum sites are representative of divergences in CH<sub>4</sub> metabolism between bog and fen habitats generally [Alstad and Whiticar, 2011; Chanton *et al.*, 2005; Galand *et al.*, 2010], suggesting that our modifications to DNDC should improve its ability to accurately simulate methanogen community dynamics and  $\delta^{13}\text{C}$  signatures of emitted CH<sub>4</sub> across northern peatlands. Acetate dynamics played an important role in predicting the contribution of CH<sub>4</sub> production pathways. For example, without acetate consumption by alternative (nonmethanogenic) processes (Figure 2), the simulated relative contribution of AM and HM to total CH<sub>4</sub> production at the Sphagnum site was about 2:1, due to substrates' (acetate and H<sub>2</sub>) availability determined by stoichiometry in CH<sub>4</sub> production processes (R1 to R3), even though  $V_{AM\_Max}:V_{HM\_Max}$  was set as 1:9, based on prior knowledge of relative abundance of methanogenic groups in this ecosystem [Bridgham *et al.*, 2013]. Acetate dynamics will also influence total CH<sub>4</sub> emissions in the current DNDC framework because acetate availability for CH<sub>4</sub> production is reduced by consumption by alternative reduction processes. Therefore, explicitly simulating acetate dynamics may be necessary for reliably simulating the contribution of AM and HM to total CH<sub>4</sub> production and CH<sub>4</sub> emissions from northern peatlands.

We note some discrepancies between the modeled results and field measurements. DNDC overestimates CH<sub>4</sub> emission rates during the early growing season (mid-June to mid-July) in 2013 at both the Sphagnum and Eriophorum sites, which may have resulted from either overpredictions of substrate availability (i.e., acetate and H<sub>2</sub>) due to relative high air temperature during this period (mean: 11.2°C from 15 June to 15 July), or oversensitivity of CH<sub>4</sub> production to temperature ( $Q_{10} = 4.6$  for CH<sub>4</sub> production) [Van Bodegom and Scholten, 2001], causing DNDC to predict relatively higher CH<sub>4</sub> production and emissions. Because meteorological data at ANS (10 km northwest of Stordalen) were used to support the simulations, and soil climate, plant growth, and CH<sub>4</sub> transformations are strongly related to temperature, deviations in predicting daily variability in CH<sub>4</sub> fluxes may in part be caused by a lack of site-specific meteorological data.

Discrepancies also exist between the modeled and observed daily  $\delta^{13}\text{C-CH}_4$  fluxes. For example, the model predicted more depleted  $^{13}\text{C}$  in emitted CH<sub>4</sub> (i.e., more negative  $\delta^{13}\text{C-CH}_4$ ) during early July to mid-August in 2012 at the Sphagnum site than in 2011 or 2013, while measured  $^{13}\text{C-CH}_4$  was less depleted in 2012 than in 2011 or 2013 (Figure 6). In the DNDC simulation, HM was a slightly larger fraction of total methanogenesis during early July to mid-August in 2012 than in 2011 or 2013 (Figure 5). DNDC results could be interpreted as a hypothesis that the relative abundance of active hydrogenotrophic methanogens would be slightly higher during early July to mid-August in 2012 than in 2011 or 2013 (Table 3 has data for 2011 only). Another possible explanation for the discrepancies between the modeled and measured  $\delta^{13}\text{C-CH}_4$  at the Sphagnum site could be discrepancies in simulations of CH<sub>4</sub> oxidation and/or  $\delta^{13}\text{C}$  in soil CO<sub>2</sub> pool, considering the negligible fractionation effects for CH<sub>4</sub> transport at this moss-dominated site. This could be evaluated by comparisons between the simulated and observed  $\delta^{13}\text{C}$  in the soil CO<sub>2</sub> pool.

Several new parameters were estimated by calibrating the simulations with the field observations in 2011 due to a lack of specific parameter values in the literature (Table 1). Most of the parameters estimated from the calibration were comparable with ranges in published data for similar ecosystem types. For example, the maximum rate of total CH<sub>4</sub> production (8.0 mmol kg<sup>-1</sup> dry peat d<sup>-1</sup>) was within the range reported for pan-Arctic Graminoid [Treat *et al.*, 2015]. However, little information can be found for the parameters  $V_{Max\_DOC}$ ,  $K_{AnDecom}$ , and  $a$ , and this lacking of parameter information suggests that some important processes regarding acetate dynamics and methanogenesis need to be better quantified. More accurate parameterization may also be helpful for improving model predictions of CH<sub>4</sub> emission. For instance, the concentration of the electron acceptors provided by humic substances is assumed to be linearly proportional to DOC concentration, and the proportionality constant has been set to one value for each type of vegetation community by constraining this parameter against the observed pore-water CO<sub>2</sub>:CH<sub>4</sub> ratio. This simplification could reflect a general characteristic of the test sites, but may be not enough to capture daily variability in the concentration of the alternative electron acceptors because the proportionality constant may actually vary across a growing season [e.g., Heitmann *et al.*, 2007]. Since acetate consumption due to the EТАH pathway is a process directly competing with AM in the model, this

constant proportionality assumption may have a notable impact on the daily variability of the simulated CH<sub>4</sub> emissions, and needs further testing.

### Acknowledgments

This study was supported by the U.S. Department of Energy (DE-SC0004632 and DE-SC0010580), the U.S. National Science Foundation (MacroSystems Biology 1241937), and the Northern Ecosystems Research for undergraduates REU Site (NSF EAR#1063037). We would like to thank all the field support students and staff. Patrick Crill was supported by Vetenskaprådet (DRF2007–4547 and 2013–5562). We thank the Abisko Scientific Research Station for providing the meteorological data, and research and logistical support during field seasons. We thank Nigel Roulet and one anonymous reviewer for helpful comments on an earlier draft. The data used to validate the model can be obtained from the publications by McCalley et al. [2014]. The model input files and outputs presented in this study are archived at Institute for the Study of Earth, Oceans, and Space, University of New Hampshire (<ftp://mire.sr.unh.edu/>).

### References

- Åkerman, H. J., and M. Johansson (2008), Thawing permafrost and thicker active layers in sub-arctic Sweden, *Permafrost Periglac.*, 19, 279–292.
- Alstad, K. P., and M. J. Whiticar (2011), Carbon and hydrogen isotope ratio characterization of methane dynamics for Flux net Peatland Ecosystems, *Org. Geochem.*, 42(5), 548–558.
- Avis, C. A., A. J. Weaver, and K. J. Meissner (2011), Reduction in areal extent of high-latitude wetlands in response to permafrost thaw, *Nat. Geosci.*, 4, 444–448.
- Bäckstrand, K., P. M. Crill, M. Mastepanov, T. R. Christensen, and D. Bastviken (2008), Total hydrocarbon flux dynamics at a subarctic mire in northern Sweden, *J. Geophys. Res.*, 113, G03026, doi:10.1029/2008JG000703.
- Bäckstrand, K., P. M. Crill, M. Jackowicz-Korczyński, M. Mastepanov, T. R. Christensen, and D. Bastviken (2010), Annual carbon gas budget for a subarctic peatland, Northern Sweden, *Biogeosciences*, 7, 95–108, doi:10.5194/bg-7-95-2010.
- Bridgman, S. D., H. Cadillo-Quiroz, J. K. Keller, and Q. Zhuang (2013), Methane emissions from wetlands: Biogeochemical, microbial, and modeling perspectives from local to global scales, *Global Change Biol.*, 19(5), 1325–1346.
- Callaghan, T. V., F. Bergholm, T. R. Christensen, C. Jonasson, U. Kokfelt, and M. Johansson (2010), A new climate era in the sub-Arctic: Accelerating climate changes and multiple impacts, *Geophys. Res. Lett.*, 37, L14705, doi:10.1029/2009GL042064.
- Chanton, J. P., G. J. Whiting, N. E. Blair, C. W. Lindau, and P. K. Bollich (1997), Methane emission from rice: Stable isotopes, diurnal variations, and CO<sub>2</sub> exchange, *Global Biogeochem. Cycles* 11, 15–27.
- Chanton, J. P., L. Chasar, P. H. Glaser, and D. I. Siegel (2005), Carbon and hydrogen isotopic effects in microbial methane from terrestrial environments, in *Stable Isotopes and Biosphere-Atmosphere Interactions: Processes and Biological Controls*, edited by L. B. Flanagan, J. R. Ehleringer, and D. E. Pataki, pp. 85–105, Elsevier, Amsterdam.
- Christensen, T. R., T. Johansson, H. J. Åkerman, M. Mastepanov, N. Malmer, T. Friberg, P. M. Crill, and B. H. Svensson (2004), Thawing subarctic permafrost: Effects on vegetation and methane emissions, *Geophys. Res. Lett.*, 31, L04501, doi:10.1029/2003GL018680.
- Conrad, R. (1989), Control of methane production in terrestrial ecosystems, in *Exchange of Trace Gases Between Terrestrial Ecosystems and the Atmosphere*, edited by M. O. Andreae and D. S. Schimel, pp. 39–58, John Wiley, New York.
- Conrad, R. (1999), Contribution of hydrogen to methane production and control of hydrogen concentrations in methanogenic soils and sediments, *FEMS Microbiol. Ecol.*, 28(3), 193–202.
- Conrad, R. (2005), Quantification of methanogenic pathways using stable carbon isotopic signatures: A review and a proposal, *Org. Geochem.*, 36(5), 739–752.
- Corbett, J. E., M. M. Tfaily, D. J. Burdige, W. T. Cooper, P. H. Glaser, and J. P. Chanton (2013), Partitioning pathways of CO<sub>2</sub> production in peatlands with stable carbon isotopes, *Biogeochemistry*, 114(1–3), 327–340.
- Deng, J., C. Li, S. Frolking, Y. Zhang, K. Bäckstrand, and P. Crill (2014), Assessing effects of permafrost thaw on C fluxes based on multiyear modeling across a permafrost thaw gradient at Stordalen, Sweden, *Biogeosciences*, 11, 4753–4770, doi:10.5194/bg-11-4753-2014.
- Deng, J., C. Li, and S. Frolking (2015), Modeling impacts of changes in temperature and water table on C gas fluxes in an Alaskan peatland, *J. Geophys. Res. -Biogeosci.*, 120, 1279–1295, doi:10.1002/2014JG002880.
- Dorrepaal, E., S. Toet, R. S. P. van Logtestijn, E. Swart, M. J. van de Weg, T. V. Callaghan, and R. Aerts (2009), Carbon respiration from subsurface peat accelerated by climate warming in the subarctic, *Nature*, 460, 616–619.
- Duddleston, K. N., M. A. Kinney, R. P. Kiene, and M. E. Hines (2002), Anaerobic microbial biogeochemistry in a northern bog: Acetate as a dominant metabolic end product, *Global Biogeochem. Cycles*, 16(4), 1063, doi:10.1029/2001GB001402.
- Ehleringer, J. R., N. Buchmann, and L. B. Flanagan (2000), Carbon isotope ratios in belowground carbon cycle processes, *Ecol. Appl.*, 10(2), 412–422.
- Eppinga, M. B., P. C. De Ruiter, M. J. Wassen, and M. Rietkerk (2009), Nutrients and hydrology indicate the driving mechanisms of peatland surface patterning, *Am. Nat.*, 173(6), 803–818.
- Frolking, S., J. Talbot, M. Jones, C. C. Treat, J. B. Kauffman, E. S. Tuittila, and N. T. Roulet (2011), Peatlands in the Earth's 21st century climate system, *Environ. Rev.*, 19, 371–396.
- Fumoto, F., K. Kobayashi, C. Li, K. Yagi, and T. Hasegawa (2008), Revising a process-based biogeochemistry model (DNDC) to simulate methane emission from rice paddy fields under various residue management and fertilizer regimes, *Global Change Biol.*, 14, 382–402.
- Galand, P. E., K. Yrjälä, and R. Conrad (2010), Stable carbon isotope fractionation during methanogenesis in three boreal peatland ecosystems, *Biogeosciences*, 7(11), 3893–3900, doi:10.5194/bg-7-3893-2010.
- Gorham, E. (1991), Northern peatlands: Role in the carbon cycle and probable responses to climatic warming, *Ecol. Appl.*, 1, 182–195.
- Graham, D. E., et al. (2012), Microbes in thawing permafrost: The unknown variable in the climate change equation, *ISME J.*, 6(4), 709–12, doi:10.1038/ismej.2011.163.
- Graham, E. B., W. R. Wieder, J. W. Leff, S. R. Weintraub, A. R. Townsend, C. C. Cleveland, L. Philpot, and D. R. Nemerugut (2014), Do we need to understand microbial communities to predict ecosystem function? A comparison of statistical models of nitrogen cycling processes, *Soil Biol. Biochem.*, 68, 279–282, doi:10.1016/j.soilbio.2013.08.023.
- Hayes, J. M. (1993), Factors controlling <sup>13</sup>C contents of sedimentary organic compounds: Principles and evidence, *Mar. Geol.*, 113(1), 111–125.
- Heitmann, T., T. Goldhammer, J. Beer, and C. Blodau (2007), Electron transfer of dissolved organic matter and its potential significance for anaerobic respiration in a northern bog, *Global Change Biol.*, 13(8), 1771–1785.
- Hodgkins, S. B., M. M. Tfaily, C. K. McCalley, T. A. Logan, P. M. Crill, S. R. Saleska, V. I. Rich, and J. P. Chanton (2014), Changes in peat chemistry associated with permafrost thaw increase greenhouse gas production, *Proc. Natl. Acad. Sci. U. S. A.*, 111(16), 5819–5824.
- Hodgkins, S. B., J. P. Chanton, L. C. Langford, C. K. McCalley, S. R. Saleska, V. I. Rich, P. M. Crill, and W. T. Cooper (2015), Soil incubations reproduce field methane dynamics in a subarctic wetland, *Biogeochemistry*, 126(1–2), 241–249.
- IPCC (2013), Climate Change 2013: The Physical Science Basis, Contribution of Working Group I to the Fifth Assessment Report of the Intergovernmental Panel on Climate Change, Cambridge University Press, Cambridge, U. K. and New York, N. Y.
- James, M., A. G. Lewkowicz, S. L. Smith, and C. M. Miceli (2013), Multi-decadal degradation and persistence of permafrost in the Alaska Highway corridor, northwest Canada, *Environ. Res. Lett.*, 8, 045013, doi:10.1088/1748-9326/8/4/045013.

- Johansson, T., N. Malmer, P. M. Crill, T. Friborg, J. Åkerman, M. Mastepanov, and T. R. Christensen (2006), Decadal vegetation changes in a northern peatland, greenhouse gas fluxes and net radiative forcing, *Global Change Biol.*, 12, 2,352–2,369, doi:10.1111/j.1365-2486.2006.01267.x.
- Johnston, C. E., S. A. Ewing, J. W. Harden, R. K. Varner, K. P. Wickland, J. C. Koch, C. C. Fuller, K. Manies, and M. T. Jorgenson (2014), Effect of permafrost thaw on CO<sub>2</sub> and CH<sub>4</sub> exchange in a western Alaska peatland chronosequence, *Environ. Res. Letts.*, 9, 085004, doi:10.1088/1748-9326/9/8/085004.
- Li, C. (2000), Modeling trace gas emissions from agricultural ecosystems, *Nutr. Cycl. Agroecosyst.*, 58, 259–276, doi:10.1023/A:1009859006242.
- Li, C. (2007), Quantifying greenhouse gas emissions from soils: Scientific basis and modeling approach, *Soil Sci. Plant Nutr.*, 53, 344–352.
- Li, C., S. Frolking, and T. A. Frolking (1992a), A model of nitrous oxide evolution from soil driven by rainfall events: 1. Model structure and sensitivity, *J. Geophys. Res.*, 97, 9759–9776.
- Li, C., S. Frolking, and T. A. Frolking (1992b), A model of nitrous oxide evolution from soil driven by rainfall events: 2. Model applications, *J. Geophys. Res.*, 97, 9777–9783.
- Li, C., J. Aber, F. Stange, K. Butterbach-Bahl, and H. Papen (2000), A process-oriented model of N<sub>2</sub>O and NO emissions from forest soils: 1. Model development, *J. Geophys. Res.*, 105, 4365–4384.
- Li, C., A. Mosier, R. Wassmann, Z. Cai, X. Zheng, Y. Huang, H. Tsuruta, J. Boonjawat, and R. Lantin (2004), Modeling greenhouse gas emissions from rice-based production systems: Sensitivity and upscaling, *Global Biogeochem. Cycles*, 18, GB1043, doi:10.1029/2003GB002045.
- Li, C., W. Salas, R. Zhang, C. Krauter, A. Rotz, and F. Mitloehner (2012), Manure-DNDC: A biogeochemical process model for quantifying greenhouse gas and ammonia emissions from livestock manure systems, *Nutr. Cycl. Agroecosyst.*, 93, 163–200, doi:10.1007/s10705-012-9507-z.
- Limpens, J., F. Berendse, C. Blodau, J. G. Canadell, C. Freeman, J. Holden, N. Roulet, H. Rydin, and G. Schaepman-Strub (2008), Peatlands and the carbon cycle: from local processes to global implications—a synthesis, *Biogeosciences*, 5, 1475–1491, doi:10.5194/bg-5-1475-2008.
- Lovley, D. R., J. D. Coates, E. L. Blunt-Harris, E. J. Phillips, and J. C. Woodward (1996), Humic substances as electron acceptors for microbial respiration, *Nature*, 382(6590), 445–448.
- Lund, M., et al. (2010), Variability in exchange of CO<sub>2</sub> across 12 northern peatland and tundra sites, *Global Change Biol.*, 16, 2436–2448.
- Malmer, N., T. Johansson, M. Olsrud, and T. R. Christensen (2005), Vegetation, climatic changes and net carbon sequestration in a North-Scandinavian subarctic mire over 30 years, *Global Change Biol.*, 11, 1895–1909.
- McCalley, C. K., et al. (2014), Methane dynamics regulated by microbial community response to permafrost thaw, *Nature*, 514(7523), 478–481.
- McGuire, A. D., L. G. Anderson, T. R. Christensen, S. Dallimore, L. Guo, D. J. Hayes, M. Helmann, T. D. Lorenson, R. W. Macdonald, and N. Roulet (2009), Sensitivity of the carbon cycle in the Arctic to climate change, *Ecol. Monogr.*, 79, 523–555.
- Melton, J. R., et al. (2013), Present state of global wetland extent and wetland methane modelling: Conclusions from a model intercomparison project (WETCHIMP), *Biogeosciences*, 10, 753–788.
- Mondav, R., et al. (2014), Discovery of a novel methanogen prevalent in thawing permafrost, *Nat. Commun.*, 5, 3212, doi:10.1038/ncomms4212.
- Nearing, M. A., L. Deer-Ascough, and J. M. Lafren (1990), Sensitivity analysis of the WEPP hillslope profile erosion model, *Trans. ASAE*, 33(3), 839–849.
- Olefeldt, D., and N. T. Roulet (2012), Effects of permafrost and hydrology on the composition and transport of dissolved organic carbon in a subarctic peatland complex, *J. Geophys. Res.*, 117, G01005, doi:10.1029/2011JG001819.
- Olefeldt, D., M. R. Turetsky, P. M. Crill, and A. D. McGuire (2013), Environmental and physical controls on northern terrestrial methane emissions across permafrost zones, *Global Change Biol.*, 19, 589–603.
- Payette, S., A. Delwaide, M. Caccianiga, and M. Beauchemin (2004), Accelerated thawing of subarctic peatland permafrost over the last 50 years, *Geophys. Res. Lett.*, 31, L18208, doi:10.1029/2004GL020358.
- Quinton, W., M. Hayashi, and L. Chasmer (2011), Permafrost-thaw-induced land-cover change in the Canadian subarctic: Implications for water resources, *Hydrol. Processes*, 25, 152–158.
- Rosswall, T., J. G. K. Flower-Ellis, L. G. Johansson, S. Jonsson, B. E. Rydén, and M. Sonesson (1975), Stordalen (Abisko), Sweden, *Ecol. Bull.*, 20, 265–294.
- Sachs, T., M. Giebels, J. Boike, and L. Kutzbach (2010), Environmental controls of CH<sub>4</sub> emission from polygonal tundra on the micro-site scale, Lena River Delta, Siberia, *Global Change Biol.*, 16, 3096–3110.
- Schneider von Diemling, T., M. Meinshausen, A. Levermann, V. Huber, K. Frieler, D. M. Lawrence, and V. Brovkin (2012), Estimating the near-surface permafrost-carbon feedback on global warming, *Biogeosciences*, 9, 649–665.
- Schuur, E. A. G., et al. (2008), Vulnerability of permafrost carbon to climate change: Implications for the global carbon cycle, *BioScience*, 58, 701–714.
- Schuur, E. A. G., J. G. Vogel, K. G. Grummer, H. Lee, J. O. Sickman, and T. E. Osterkamp (2009), The effect of permafrost thaw on old carbon release and net carbon exchange from tundra, *Nature*, 459, 556–559.
- Schuur, E. A. G., A. Benjamin, and Permafrost Carbon Network (2011), High risk of permafrost thaw, *Nature*, 480, 32–33.
- Segers, R., and S. W. M. Kengen (1998), Methane production as a function of anaerobic carbon mineralization: A process model, *Soil Biol. Biochem.*, 30(8), 1107–1117.
- Tarnocai, C., J. G. Canadell, E. A. G. Schuur, P. Kuhry, G. Mazhitova, and S. Zimov (2009), Soil organic carbon pools in the northern circumpolar permafrost region, *Global Biogeochem. Cycles*, 23, GB2023, doi:10.1029/2008GB003327.
- Treat, C. C., et al. (2015), A pan-Arctic synthesis of CH<sub>4</sub> and CO<sub>2</sub> production from anoxic soil incubations, *Global Change Biol.*, 21, 2787–2803, doi:10.1111/gcb.12875.
- Van Bodegom, P. M., and J. C. Scholten (2001), Microbial processes of CH<sub>4</sub> production in a rice paddy soil: Model and experimental validation, *Geochim. Cosmochim. Acta*, 65(13), 2055–2066.
- Wania, R., I. Ross, and I. C. Prentice (2009a), Integrating peatlands and permafrost into a dynamic global vegetation model: 1. Evaluation and sensitivity of physical land surface processes, *Global Biogeochem. Cycles*, 23, GB3014, doi:10.1029/2008GB003412.
- Wania, R., I. Ross, and I. C. Prentice (2009b), Integrating peatlands and permafrost into a dynamic global vegetation model: 2. Evaluation and sensitivity of vegetation and carbon cycle processes, *Global Biogeochem. Cycles*, 23, GB3015, doi:10.1029/2008GB003413.
- Wania, R., et al. (2013), Present state of global wetland extent and wetland methane modelling: Methodology of a model inter-comparison project (WETCHIMP), *Geosci. Model Dev.*, 6(3), 617–641.

- Wieder, W. R., G. B. Bonan, and S. D. Allison (2013), Global soil carbon projections are improved by modelling microbial processes, *Nat. Clim. Change*, 3, 909–912, doi:10.1038/NCLIMATE1951.
- Xu, X., F. Yuan, P. J. Hanson, S. D. Wullschleger, P. E. Thornton, W. J. Riley, X. Song, D. E. Graham, C. Song, and H. Tian (2016), Reviews and syntheses: Four decades of modeling methane cycling in terrestrial ecosystems, *Biogeosciences*, 13, 3735–3755, doi:10.5194/bg-13-3735-2016.
- Yu, Z., J. Loisel, D. P. Brosseau, D. W. Beilman, and S. J. Hunt (2010), Global peatland dynamics since the Last Glacial Maximum, *Geophys. Res. Lett.*, 37, L13402, doi:10.1029/2010GL043584.
- Zhang, Y., C. Li, C. C. Trettin, H. Li, and G. Sun (2002), An integrated model of soil, hydrology and vegetation for carbon dynamics in wetland ecosystems, *Global Biogeochem. Cycles*, 16(4), 1061, doi:10.1029/2001GB001838.
- Zhang, Y., T. Sachs, C. Li, and J. Boike (2012), Upscaling methane fluxes from closed chambers to eddy covariance based on a permafrost biogeochemistry integrated model, *Global Change Biol.*, 18, 1428–1440, doi:10.1111/j.1365-2486.2011.02587.x.
- Zhuang, Q., V. E. Romanovsk, and A. D. McGuire (2001), Incorporation of a permafrost model into a large-scale ecosystem model: Evaluation of temporal and spatial scaling issues in simulating soil thermal dynamics, *J. Geophys. Res.*, 106, 33,649–33,670.
- Zhuang, Q., J. M. Melillo, D. W. Kicklighter, R. G. Prinn, A. D. McGuire, P. A. Steudler, B. S. Felzer, and S. Hu (2004), Methane fluxes between terrestrial ecosystems and the atmosphere at northern high latitudes during the past century: A retrospective analysis with a process-based biogeochemistry model, *Global Biogeochem. Cycles*, 18, GB3010, doi:10.1029/2004GB002239.
- Zimov, S. A., E. A. Schuur, and F. S. Chapin III (2006), Permafrost and the global carbon budget, *Science*, 312(5780), 1612–1613.